CHAPTER 3

Effect of Initial Excess Pore Water Pressure on Saturated Consolidation of Homogeneous/Layered clays

3.1 INTRODUCTION

In most of the textbooks (Terzaghi 1943; Holtz and Kovacs 1981; Berry and Reid 1988) as well as in engineering practices, the transient flow of water through the soils is analysed by considering the rectangular (uniform) distribution of u_0. The assumption of uniform distribution of u_0 is reasonable for a thin consolidating layer subjected to an external load having a large contact area (e.g. an embankment or earthen dam resting on impervious soil, tunnel, and water gallery passing through the soil, deep foundation resting on clay underlain by pervious layer, etc.). Nevertheless, shallow foundations often face a contrary scenario in which a finite surface area is loaded on top of a large clay layer. This arrangement can result in a range of uneven pore water pressure patterns, ranging from linearly decreasing and trapezoidal to exponentially decaying and beyond. The self-weight of slurry in fine-grained hydraulic fill also gives rise to linearly increasing u_0. Upon the application of external load on a clayey layer that had already undergone a certain amount of consolidation, due to its self-weight or previously applied loading and unloading, it will be quite sensible to start the analysis by adopting sinusoidal/parabolic or half sinusoidal shaped u_0 depending on the drainage boundary conditions. Considering the side friction of the wall, Lovisa and Shivakugan (2014) used classical arching theory to assume the initial excess PWP of tall samples (height>40% of diameter) in the oedometer test. Each of these non-uniform patterns can significantly impact settlement calculations, resulting in various

outcomes that must be meticulously taken into account during geotechnical evaluations and planning procedures.

Nevertheless, most of the settlement studies are still performed with uniform u_0 distribution despite the contradicting empirical evidence. Various researchers (Janbu *et al.* 1956; Darrag and Tawil 1993; Singh 2005, 2007; Singh and Swamee 2008; Lovisa *et al.* 2010, 2012; Lovisa and Shivakugan 2014) also carried out analytical studies of consolidation for one- and two-way drainage layer by assuming several other forms of initial excess PWP distributions (e.g. linearly increasing/ decreasing, parabolic, sinusoidal). With the assumptions of linearly increasing (basic triangular loading) and linearly decreasing (reverse triangular loading) u_0 distribution, Terzaghi and Frohlich (1936) and Janbu *et al.* (1956) analyzed the consolidating behaviour of clayey stratum having freely drainage surface at the top and impervious surface at the bottom. Considering the variability of the soil and the loading conditions, Darrag and Tawil (1993) studied a one-dimensional consolidation equation considering a stochastic Gaussian initial excess PWP. Singh (2005) further obtained the analytical expressions for the consolidating curve corresponding to the distribution of u_0 through basic and reverse triangular loadings. Corresponding to the two-way drainage layer, Singh (2007) estimated the coefficient of consolidation by the diagnostic curve method. Singh and Swamee (2008) analyzed the consolidating curves for basic and reverse triangular loadings and subsequently proposed the approximate equations for representing the time variation of consolidation, both explicitly and implicitly. Lovisa *et al*. (2010) investigated the effect of few distributions on the consolidation behavior of soil stratum subjected to both-way drainage by series solution method. They proposed an alternative method of consolidation analysis by normalizing the isochrones with respect to the maximum value of initial excess PWP (u_{0max}). Lovisa *et al*. (2012) further extended their work for consolidating layer subjected to one-way drainage.

Lovisa and Shivakugan (2015) reported the analytical solutions of U_{avg} for six different distributions of u_0. In all these series solutions, special attention is required to eliminate the oscillatory effects that emerge at the discontinuity due to the Gibbs phenomenon (Carslaw 1930). One-dimensional consolidation analysis is also carried out by various numerical methods, especially the finite element method (Christian and Boehmer 1970, Abid and Pyrah 1988, Huang and Griffiths 2010). Nevertheless, the numerical solutions for one-dimensional consolidation with a wide range of u_0 distribution seem to be unaddressed.

Conventionally, the consolidation analysis is carried out for the homogenous clays. However, in many projects, a clayey stratum consists of a series of layers having different permeability and compressibility properties. Several researchers (Gray 1945; Schiffmann and Stein 1970; Takada and Mikasa 1984; Lee et al. 1992; Pyrah 1966; Yuan-qiang et al. 2004; Zhu 2005; Huang 2010; Kim and Mission 2011; Zhang et al. 2015) predicted the consolidation phenomenon in the layered clays by analytical approaches with the rectangular distribution of u_0. They reported that the material properties (e.g. permeability, compressibility) and the thickness of each layer play a vital role in governing the overall consolidation behavior of the clayey stratum. However, no work seems to exist where the consolidation of two-layered clays is provided by considering the various shapes of u_0 distributions.

The present chapter depicts numerical insights to elaborate on the impact of various u_0-profiles on the overall consolidation behaviour. There are two parts of this chapter- the first part deals with the homogenous clays and the second part focuses on the layered clays. The one-dimensional linear consolidation analysis is carried out by considering two different sets of drainage boundaries– (i) Pervious top and pervious bottom (PTPB) and (ii) Pervious top and impervious bottom (PTIB). A total number of ten different forms of u_0-distributions (symmetric/asymmetric, linear/non-linear) are considered. A series of

numerical simulations are performed by changing the variables of each u_0-distribution, as well as the material parameters, and the layer thickness. The Crank-Nicolson implicit scheme of the finite difference method is employed for executing the numerical simulations. A detailed comparative study is presented to show the difference between different u_0 distributions and the deviation of the evaluated numerical solutions from their analytical counterparts. The results are shown in terms of normalized isochrones (i.e. the spatial trajectory of the pore water pressure), consolidation curves, and the trace of maximum PWP within the consolidating layers.

3.2 ASSUMED DISTRIBUTION OF INITIAL EXCESS PORE WATER PRESSURE

Fig. 3.1 describes all the forms of assumed distributions of u_0 considered in the present analysis. Ten different u_0 distributions (Case A - Case J) are chosen. The grey shaded area displays the u_0 loading generated instantaneously at the time of load application. The curves are drawn between two non-dimensional parameters, namely, normalized depth, Z (=z/H), and normalized u_0 (u_0/u_{0max}); where, D_p =drainage path, and u_{0max} (maximum u_0) = q. The vertical and horizontal axes represent Z and u_0/q, respectively. The maximum value in the horizontal scale always remains to be 1. The value of Z at the bottom layer (denoted by z_1) for one- and two-way drainage becomes equal to 1 and 2, respectively.

The curves (symmetric/asymmetric) displayed in Fig. 3.1 are not arbitrary. For a specific situation where a consolidating clay layer is sandwiched between two sandy layers, a triangular u_0 distribution is likely to develop in the field due to the occurrence of either of the two conditions: (i) if there is a sudden rise/drop of the water surface in the upper sand while the piezometric level of the bottom layer is unaltered (Lambe and Whitman, 1969) or (ii) if the lower sand layer is suddenly dewatered by destruction of an artesian condition

without changing the water table at the upper sand (Olson, 1980). Based on the hydraulic drainage and environmental conditions, upper/lower triangular distribution may evolve. A trapezoidal distribution is the combination of the rectangular and triangular surfaces. The composite shape, as shown in Fig. 3.1a, is a combination of rectangular and parabolic/sinusoidal distribution. Figs. 3.1b-3.1d represent the linear distribution of u_0 loading. Fig. 3.1e represents the sinusoidal distribution of u_0 with u_{0max} at the mid portion and zero pore pressure at both boundaries. The sinusoidal distribution can be because of the fill applied at some previous time. Figs. 3.1f-3.1h display other variants of the fundamental sinusoidal distribution. The skewed distribution (top-skewed/ bottom-skewed) can arise after a certain degree of consolidation takes place from linear triangular u_0 surface developed due to the previously placed fill, whereas the arched distribution occurs for relatively tall samples in the oedometer test due to the effect of skin friction. The shapes of all the considered distributions are mathematically expressed by the following normalized equation:

1) **Parabolic Distribution (Fig. 3.1a)**

$$\frac{u_0}{u_{0\max}} = \frac{4z(1-b_1)(H-z)+b_1H^2}{H^2} \qquad (3.1)$$

2) **Triangular Distribution (Fig. 3.1b)**

$$\frac{u_0}{u_{0\max}} = \frac{Z}{b_2} \qquad 0 \le Z \le b_2 \qquad (3.2a)$$

$$= \frac{(z_1 - Z)}{(z_1 - b_2)} \qquad b_2 \le Z \le 1 \qquad (3.2b)$$

Here, b_2 (i.e., the normalized distance of the apex from the top surface) varies between 0 and 1; where, $b_2 = 0$ (basic triangular loadings), and $b_2 = 1$ (reverse triangular loadings).

3) **Trapezoidal Distribution**
   a) Shorter base on the vertical-axis (Fig. 3.1c)

$$\frac{u_0}{u_{0\max}} = \frac{2Z}{z_1 - b_3} \qquad 0 \le Z < \frac{z_1 - b_3}{2} \qquad (3.3a)$$

$$= 1 \qquad \frac{z_1 - b_3}{2} \le Z \le \frac{z_1 + b_3}{2} \tag{3.3b}$$

$$= \frac{2(z_1 - Z)}{(z_1 - b_1)} \qquad \frac{z_1 + b_3}{2} < Z \le z_1 \tag{3.3c}$$

b) Shorter base on the horizontal- axis (Fig. 3.1d)

$$\frac{u_0}{u_{0\max}} = \frac{Z}{z_1} + b_4\left(1 - \frac{Z}{z_1}\right) \tag{3.4}$$

Here, b_3 and b_4 (i.e., the normalized length of the shorter base) varies between 0 and 1. The triangular and rectangular distributions are implied by imposing b_3 (/b_4) = 0 and 1, respectively.

4) Different trigonometric distribution

a) Sine Distribution (Fig. 3.1e): $\frac{u_0}{u_{0\max}} = \sin\left(\frac{z\pi}{H}\right)$ (3.5a)

b) Cosine distribution (Fig. 3.1f): $\frac{u_0}{u_{0\max}} = \cos\left(\frac{z\pi}{4H}\right)$ (3.5b)

c) Half sine decreasing (Fig. 3.1g): $\frac{u_0}{u_{0\max}} = \sin\left(\frac{(z+H)\pi}{2H}\right)$ (3.5c)

d) Half sine increasing (Fig. 3.1h): $\frac{u_0}{u_{0\max}} = \sin\left(\frac{z\pi}{2H}\right)$ (3.5d)

5) Skewed distribution (Fig. 3.1i)

$$\frac{u_0}{u_{0\max}} = 10^{0.272\alpha}\left(\left(\frac{z}{H}\right)^{0.25\alpha}\left(1 - \frac{z}{H}\right)^{\alpha}\right) \qquad \text{(for } b_5\text{=0.2)} \tag{3.6a}$$

$$\frac{u_0}{u_{0\max}} = 10^{0.602\alpha}\left(\frac{z}{H}\left(1 - \frac{z}{H}\right)\right)^{\alpha} \qquad \text{(for } b_5\text{=0.5)} \tag{3.6b}$$

$$\frac{u_0}{u_{0\max}} = 10^{0.272\alpha}\left(\left(\frac{z}{H}\right)^{\alpha}\left(1 - \frac{z}{H}\right)^{0.25\alpha}\right) \qquad \text{(for} b_5\text{=0.8)} \tag{3.6c}$$

Degree of skewness (α) is adopted as 2, 10 and 20.

6) Arched distribution (Fig. 3.1j) $\frac{u_0}{u_{0\max}} = \exp^{-1.08\chi Z / z_1}$ (3.7)

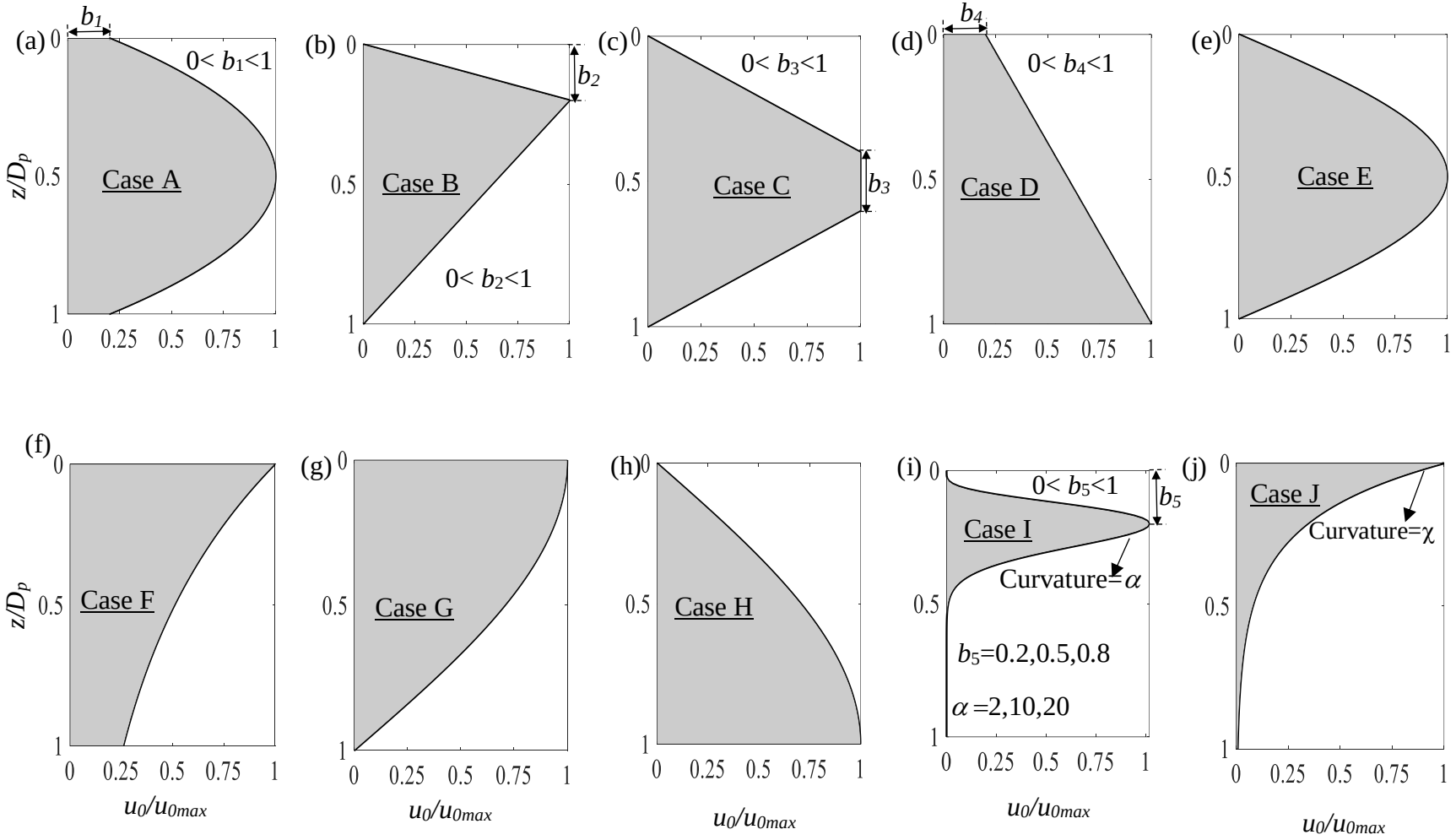

Fig. 3.1 Various shapes of the assumed u_o distribution: (a) Parabolic, (b) Triangular, (c and d) Trapezoidal, (e) Sine, (f) Cosine, (g) Half Sine Decreasing, (h)Half Sine Increasing, (i) Skewed, (j) Arched.

3.3 DEFINITION OF THE COMPUTED PARAMETERS

The obtained numerical solutions are presented in terms of isochrones, consolidating curves, and u_{max} path.

3.3.1 Isochrones

Isochrones are the curves drawn between the degree of consolidation and the depth of the consolidating layer at a certain time. Since u_0 is a function of depth, the degree of consolidation at any definitive depth (U_z) in the consolidating layer is defined as:

$$U_z = \frac{u(z,t)}{Max(u(z,0))} = \frac{u(z,t)}{u_{0max}} \tag{3.8}$$

Note that U_Z ranges between 0 and 1. A series of isochrones represents the entire consolidation process.

3.3.2 Consolidating curves (U_{avg} versus T_v relationship)

The average degree of consolidation for the entire layer (U_{avg}) is defined as the ratio of the total amount of dissipated excess PWP and the developed initial excess PWP. Mathematically, it is expressed as the following equation:

$$U_{avg} = 1 - \frac{\int_0^{layer\ thickness} u(z,t)\,dz}{\int_0^{layer\ thickness} u(z,0)\,dz} \tag{3.9}$$

It indicates the fraction of settlement a consolidating layer has experienced at any arbitrary time which is expressed in terms of non-dimensional time factor, T_v ($T_v = c_v t / D_p^2$).

3.3.3 u_{max} paths

A series of u_{max} points (i.e., the peak position of the isochrones) are joined together to obtain a locus of the maximum pore pressure points at different states of consolidation; this is termed as 'u_{max} path' in the present work. The u_{max} path gives an idea of how the

shape of the isochrones changes with the progress of consolidation and thus provides the understanding of the time frame at which the isochrones turn parabolic (for PTPB) or half parabolic (for PTIB). Instead of producing so many isochrones in one diagram, the approach of representing the consolidation phenomenon through the u_{max} path appears to be quite sensible and far more effective.

3.4 HOMOGENEOUS SOIL

3.4.1 Problem Statement

A consolidating soil layer of thickness, *H*, is subjected to a constant external load (*q*) as shown in Fig.3.2. The soil is considered to be isotropic and exhibits a uniform coefficient of consolidation (c_v). The parameter c_v relates the hydraulic conductivity (*k*) and the volume compressibility (m_v) of the soil as: $c_v = k/(m_v\gamma_w)$. It is mention-worthy that as long as c_v remains constant, variations of *k* and m_v do not make any change in the consolidation prediction. Due to the application of external load, excess pore water pressure (u_0) develops instantaneously within the soil layer. It is intended to analyze the consolidation phenomenon of the clayey layer subjected to the above-mentioned u_0 loadings considering two drainage boundary conditions- PTPB and PTIB. The drainage paths (D_p) for PTPB and PTIB are *H*/2 and *H*, respectively.

3.4.2 Mathematical formulations

The 1-D linear consolidation is assumed to be governed by the following parabolic partial differential expression (derivation in Appendix A1):

Governing Differential Equation: $$c_v \frac{\partial^2 u}{\partial z^2} = \frac{\partial u}{\partial t} \qquad (3.10)$$

where, *u* is the excess PWP at any depth from the top surface (*z*) corresponding to any arbitrary time (*t*). Here, *z* is measured positive along the vertical downward direction.

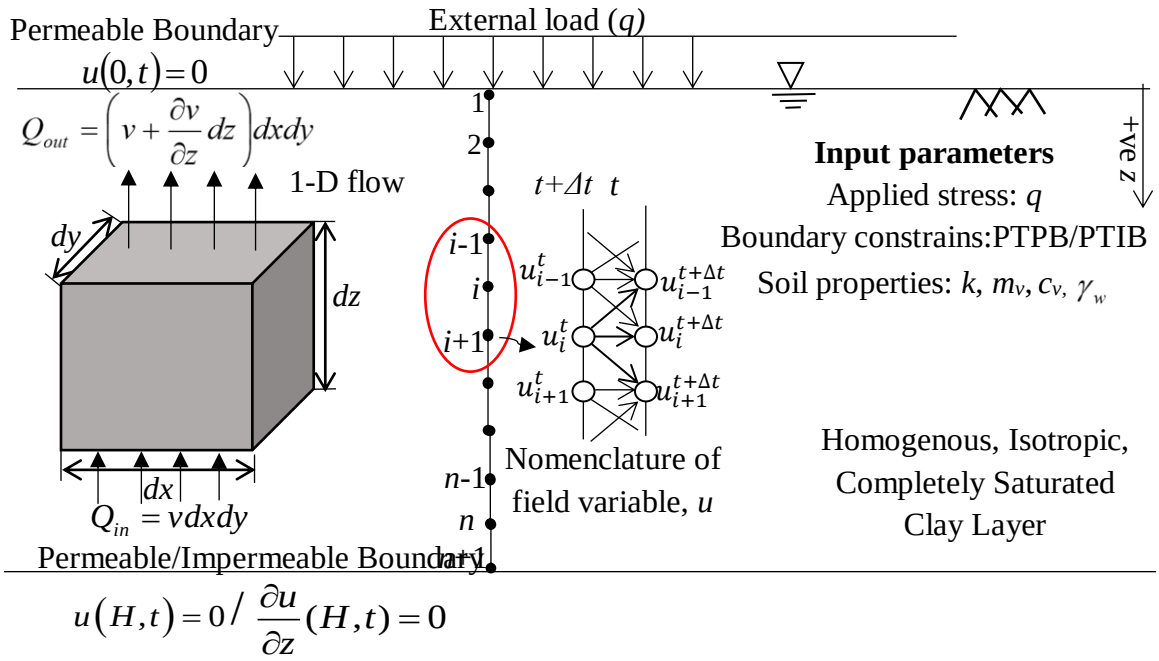

Fig. 3.2 Homogeneous consolidating stratum subjected to strip loading along with the finite difference discretization.

The problem of consolidation is an initial value problem that involves the following boundary (drainage) and initial constraints along with Eq. 3.10.

$$\text{Boundary Conditions:} \quad \begin{cases} \text{For PTPB:} \;\; u(0,t)=0 \text{ and } u(H,t)=0 \\ \text{For PTIB:} \;\; u(0,t)=0 \text{ and } \dfrac{du}{dz}(H,t)=0 \end{cases} \tag{3.11}$$

$$\text{Initial Condition:} \quad u(z,0)=u_0 \tag{3.12}$$

3.4.3 Solution Strategy

The domain is discretized with n number of segments resulting in n +1 number of grid points (also loosely referred here as nodes). Eq. 3.10 must be satisfied at each node and Eq. (3.11) needs to be satisfied at the boundary grid points. Fig. 3.2 shows the schema of the node numbering system. For any arbitrary grid point, i, Eq. 3.10 can be recast as below:

$$\left.\frac{\partial u}{\partial t}\right|_i = c_v \left.\frac{\partial^2 u}{\partial z^2}\right|_i = c_v \left[(1-\phi) \left.\frac{\partial^2 u}{\partial z^2}\right|_i^t + \phi \left.\frac{\partial^2 u}{\partial z^2}\right|_i^{t+\Delta t} \right] \tag{3.13}$$

Here, the subscript and superscript refer to the point position and the timestep, respectively; t refers to the previous timestep and $t+\Delta t$ refers to the current timestep. The second-order spatial derivative of u is decoupled in two timesteps (previous and current) by using the ϕ-parameter. Based on the value of ϕ, there are the following three finite difference schemes:

ϕ = 0.0, Explicit scheme

= 0.5, Crank Nicolson Semi-Implicit scheme

= 1.0, Fully Implicit scheme

Following the Taylor series expansion, Eq. 3.13 can be discretized as follows:

$$\frac{u_i^{t+\Delta t} - u_i^t}{\Delta t} = c_v \left(\frac{u_{i-1}^t - 2u_i^t + u_{i+1}^t}{\Delta z^2}(1-\phi) + \frac{u_{i-1}^{t+\Delta t} - 2u_i^{t+\Delta t} + u_{i+1}^{t+\Delta t}}{\Delta z^2}\phi \right) \tag{3.14a}$$

$$\Rightarrow -\lambda\phi\left(u_{i-1}^{t+\Delta t} - 2u_i^{t+\Delta t} + u_{i+1}^{t+\Delta t}\right) + u_i^{t+\Delta t} = \lambda(1-\phi)\left(u_{i-1}^t - 2u_i^t + u_{i+1}^t\right) + u_i^t \; ; \; \lambda = \frac{c_v \Delta t}{\Delta z^2} \tag{3.14b}$$

Here, (i) u_{i-1}^t, u_i^t, u_{i+1}^t are the excess PWP obtained at time t correspond to i-1, i, i+1 th point, respectively, (ii) $u_{i-1}^{t+\Delta t}$, $u_i^{t+\Delta t}$, and $u_{i+1}^{t+\Delta t}$ are the excess PWP obtained at time $t + \Delta t$ correspond to i–1, i, and i+1th point, respectively, and (iii) λ is the non-dimensional user-defined parameter.

The analysis is performed with the aid of Crank-Nicolson method (i.e., ϕ=0.5). This method provides a high order of accuracy and guarantees unconditional stability. The entire numerical simulations are performed by developing a code in *MATLAB* (version 2018). The compacted matrix of Eq. 3.14b mentioned in Appendix A2.

3.4.4 Results and Discussions

3.4.4.1 Isochrones and u_{max} path for PTPB

Fig. 3.3 presents the isochrones for PTPB corresponding to five different values of T_v, namely, 0.00, 0.02, 0.06, 0.100, and 0.200. No sooner than the consolidation process begins, 100% of the developed u_0 is assumed to dissipate at the top and the bottom boundary layers. Note that the isochrones are drawn by normalizing the excess PWP with respect to u_{0max}. It is well noted that for symmetric variation of u_0, (e.g. variations shown in Figs. 3.1a, 3.1c, 3.1e) the isochrones at any arbitrary time also remains to be symmetric. For asymmetric distributions of u_0 (e.g. Figs. 3.1b, 3.1d, 3.1f, 3.1g, 3.1h, 3.1i, 3.1j.), u_{max} points are aligned towards u_{0max} and over the time the shape of the curves gradually becomes symmetric. The u_{max} path is shown by the thick solid line in Fig. 3.3. It is observed that the u_{max} path are stepped in nature; this indicates that the time interval used in this analysis (Δt = 0.01) evolves few isochrones for which the position of u_{max} remains identical. For the skewed distribution, it is observed that in the thinner leg section of the u_0 distributions, PWP increases with time. This is attributed to the fact that the phenomenon of pore water pressure redistribution occurs within the consolidating layer resulting in increasing in excess PWP in those regions where the value of u_0 were minimal. It is to be noted in this stage that unlike the conventional approach of Terzaghi, Lovisa et al. 2010 approach of representing the consolidation behavior by the normalized isochrones captures the redistribution phenomenon aptly.

The u_{max} path for the consolidating layer subjected to various u_0 loadings are presented in Fig. 3.4. For the symmetric u_0 distributions (Cases A, C and E), the u_{max} path always remains horizontal and passes through the central portion of the consolidating layer. The u_{max} paths for Cases G and H are symmetrically opposite. By varying the apex position of the triangular u_0 distribution, the u_{max} paths are shown in Fig. 3.4 d. It is observed that

for every b_4, except b_4=0.5, the shape of isochrones become symmetric almost at the same time. The magnitude of the parameter b_4, for trapezium distribution, significantly influences the time factor at which the isochrones turn symmetric. The u_{max} path are also presented for skewed distribution to signify the influences of α and b_5.

3.4.4.2 Isochrones and u_{max} path for PTIB

Fig. 3.5 shows the normalized isochrones for the PTIB case subjected to various distributions of u_0 and corresponding to the same set of T_v as considered earlier. As expected, all isochrones (for T_v >0) meet the impervious bottom surface orthogonally. The redistribution of the excess PWP is more prominent in the PTIB condition in comparison to its PTPB counterpart. The degree of redistribution near the impervious zone increases as u_{0max} is assumed to develop away from the bottom impervious surface. This may be due to the fact that the pore water in the maximum position flows in both direction and eventually creates additional pressure. As the consolidation process progresses, this developed excess PWP starts dissipating and gradually the isochrones turn into the shape expected, all isochrones (for T_v >0) meet the impervious bottom surface orthogonally. The redistribution of the excess PWP is more prominent in the PTIB condition in comparison to its PTPB counterpart. The degree of redistribution near the impervious zone increases as u_{0max} is assumed to develop away from the bottom impervious surface. This may be due to the fact that the pore water in the maximum position flows in both directions and eventually creates additional pressure. As the consolidation process progresses, this developed excess PWP starts dissipating, and gradually, the isochrones turn into the shape of a half parabola. The u_{max} path for various distributions by varying the associated parameters (e.g. b_1, b_2, b_3) are drawn in Fig. 3.6. The figure gives a clear impression of how these parameters play an important role in governing the size and shape of the isochrones over the time.

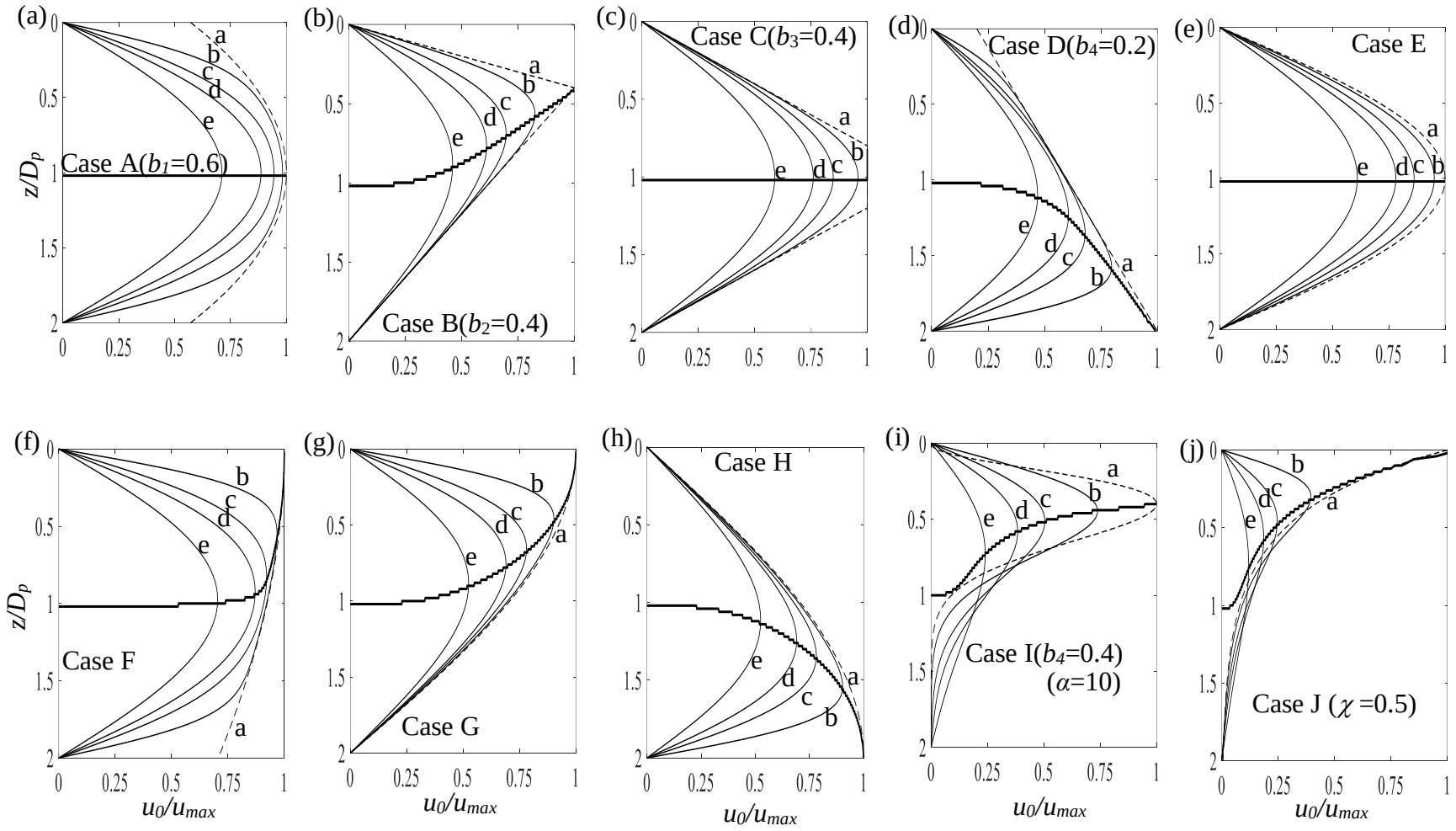

N.B.: (i) a, b, c, d and e represents the consolidating isochrones @ T_v equals to 0.000, 0.02, 0.06, 0.100, and 0.200, respectively.

(ii) Dashed line indicates the u_0 isochrones and the thick line shows the path of u_{max} within the consolidating layer over time.

Fig. 3.3 Isochrones and u_{max} path for PTPB consolidating layer subjected to various u_0 loading

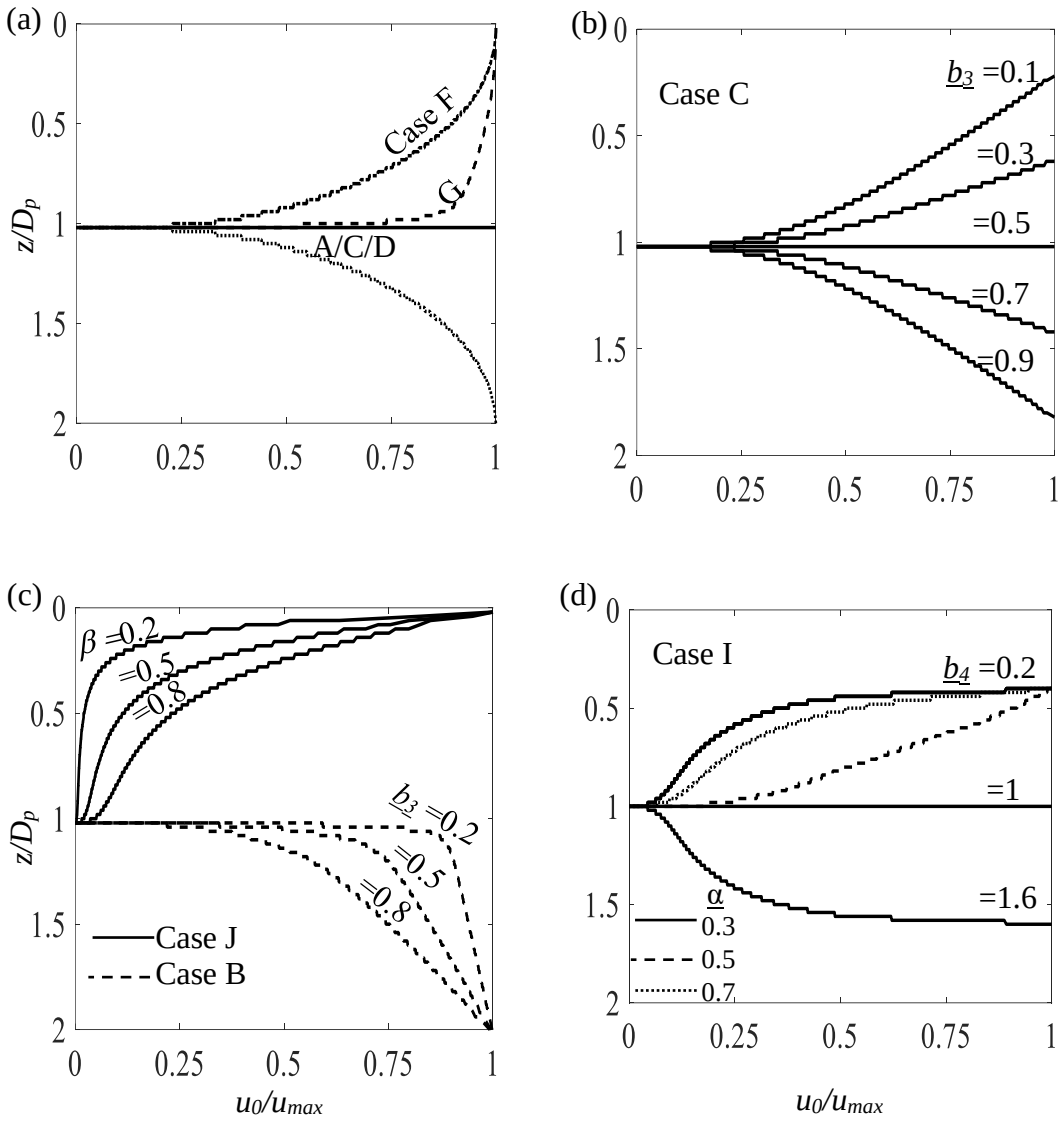

Fig. 3.4 u_{max} path for PTPB consolidating layer for various u_0 loadings and the corresponding associated variables.

3.4.4.3 U_{avg} versus T_v curves for PTPB and PTIB

Fig. 3.7 and 3.8 further depicts the variation of U_{avg} with respect to time factor for PTPB and PTIB conditions, respectively. The variations seem to be more prominent for PTIB condition. Following few observations are made from the plotted figures:

a) The magnitude of b_1 in the parabolic distribution prominently controls the shape of the U_{avg} versus T_v curve only when the consolidating layer is subjected to one-way drainage.By changing the apex position of the triangular distribution in Case B, it

can be concluded that the consolidation rate increases if the initial excess PWP is accumulated closer to any pervious surfaces (top/bottom) of the PTPB layer; whereas, if u_{0max} is close to the impervious surface of PTIB layer, the dissipation process slows down.

b) In comparison to the conventional constant u_0 distribution, the distribution in Case C slows down the rate of consolidation.

c) Variation of b_4 in Case D does not influence the consolidating curves for PTPB conditions; however, for one-way drainage the parameter b_4 affects the U_{avg} versus T_v curves markedly.

d) Comparing different trigonometric distributions, it can clearly be seen that although, the sinusoidal u_0 distribution accelerates the process of consolidation for PTPB condition, but slows down the dissipation rate for the consolidating layer subjected to one-way drainage.

e) Normalized depth of the skewed distribution from the top surface (b_5) plays a key role in influencing the nature of the consolidating curves for PTPB as well as PTIB condition in comparison to the degree of skewness (α).

f) The rate of consolidation increases if the majority of the initial excess PWP is concentrated near the drainage surface.

g) Unlike the PTIB condition, curvature of the arched distribution affects the consolidating curves for the two-way drainage layer.

h) It is observed that although the consolidation curves may be identical for different u_0 distributions however, the consolidation isochrones for each distribution are unique. Hence, the comprehensive way of representing the consolidation behavior of a clayey layer is by presenting the U_{avg} versus T_v curves along with the normalized isochrones and the u_{max} path.

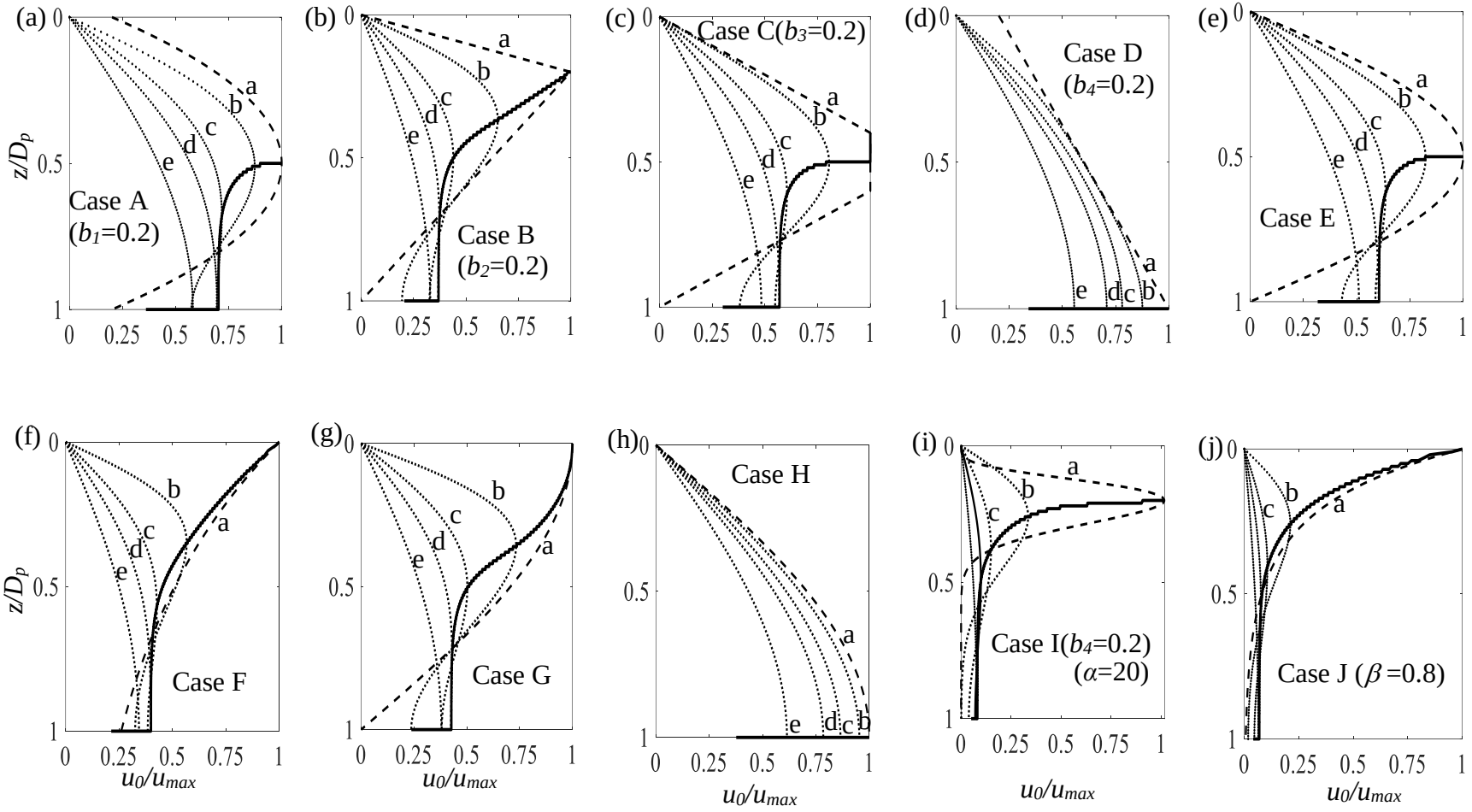

N.B.: (i) a, b, c, d and e represents the consolidating isochrones @ T_v equals to 0.000, 0.02, 0.06, 0.100, and 0.200, respectively.

(ii) Dashed line indicates the u_0 isochrones and the thick line shows the path of u_{max} within the consolidating layer over time.

Fig. 3.5 Isochrones and u_{max} path for PTIB consolidating layer subjected to various u_o loading

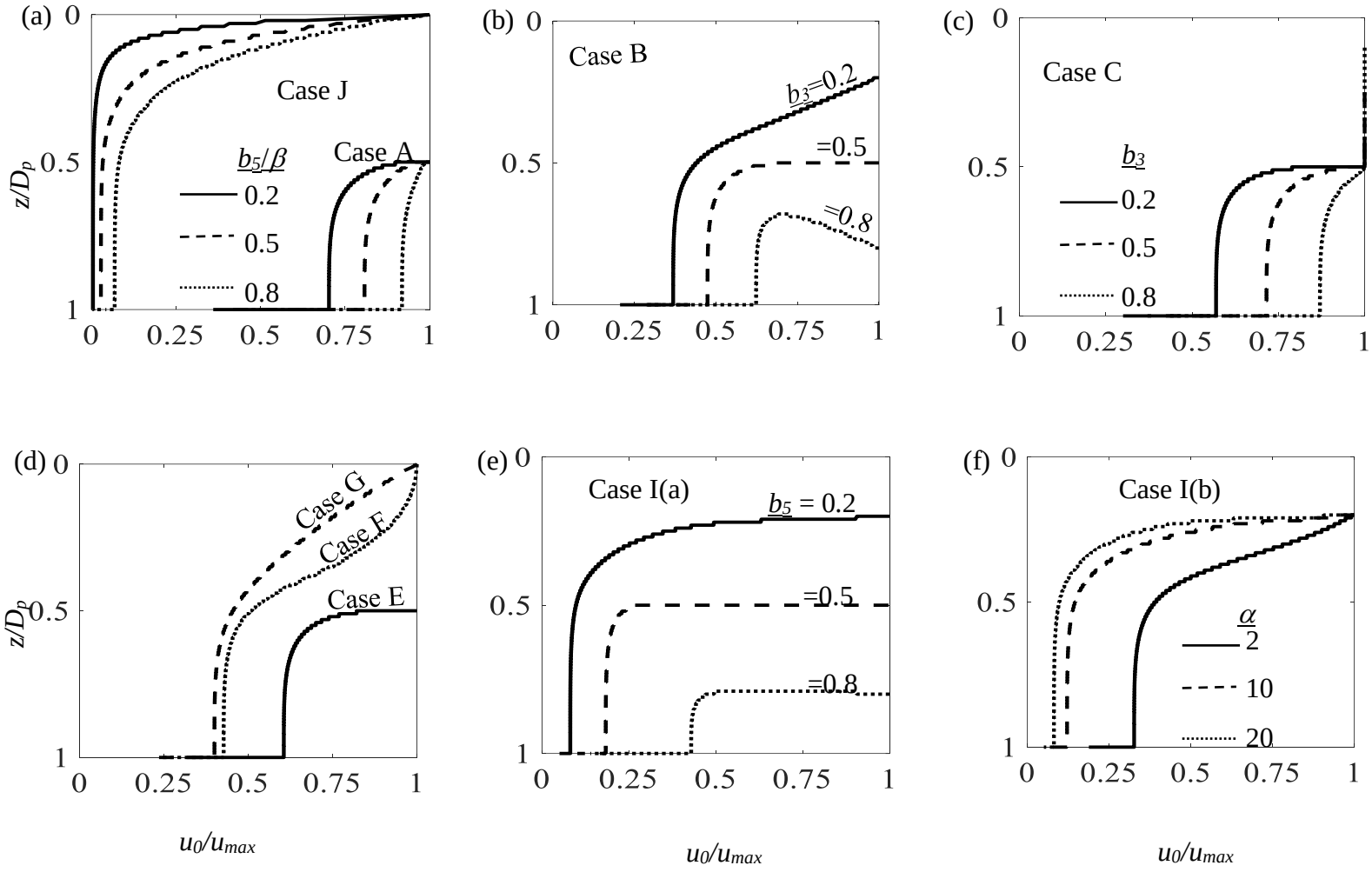

Fig. 3.6 u_{max} path for PTIB consolidating layer for various u_o loadings and the corresponding associated variable

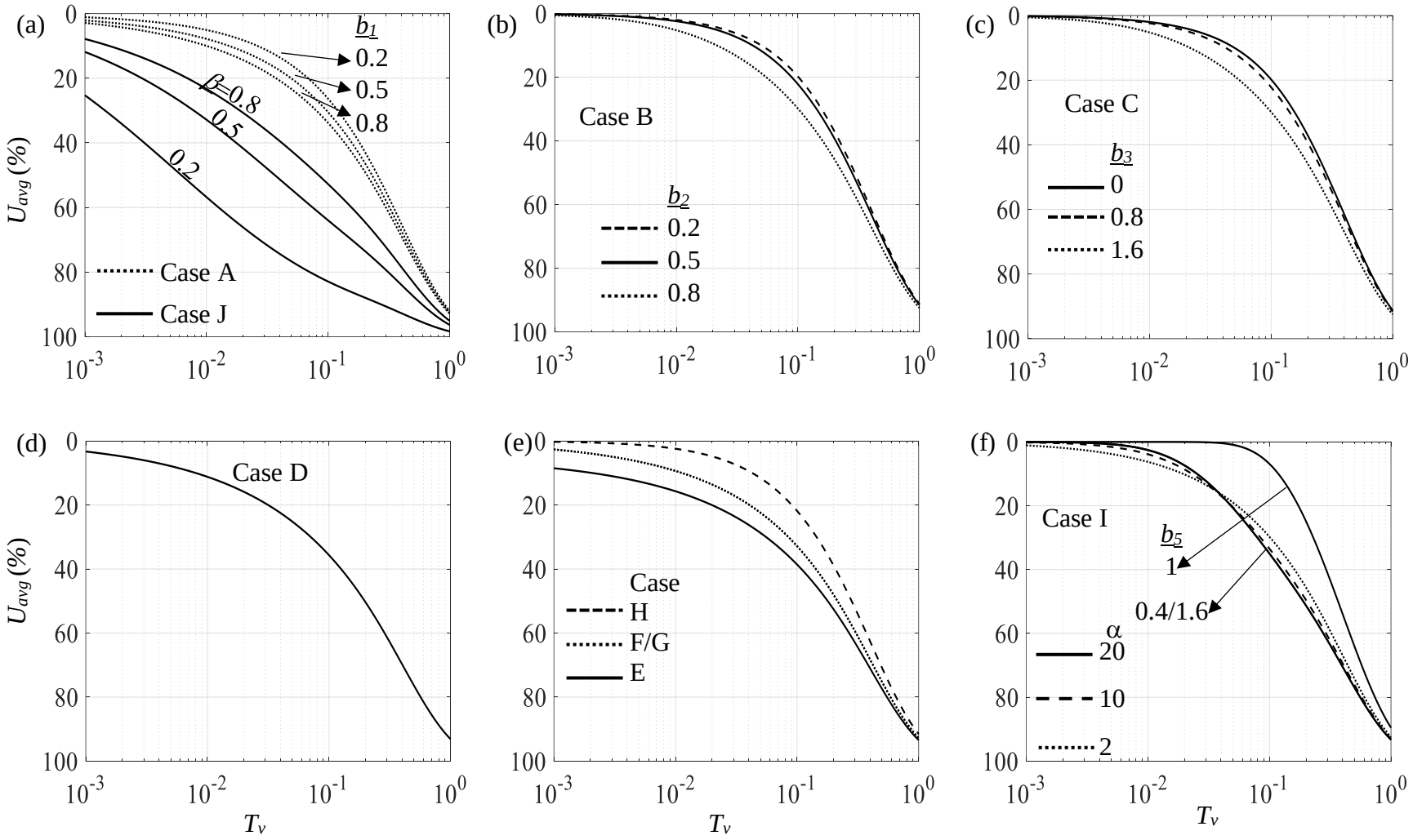

Fig. 3.7 U_{avg} versus T_v curves for the consolidating layer subjected to two-way drainage.

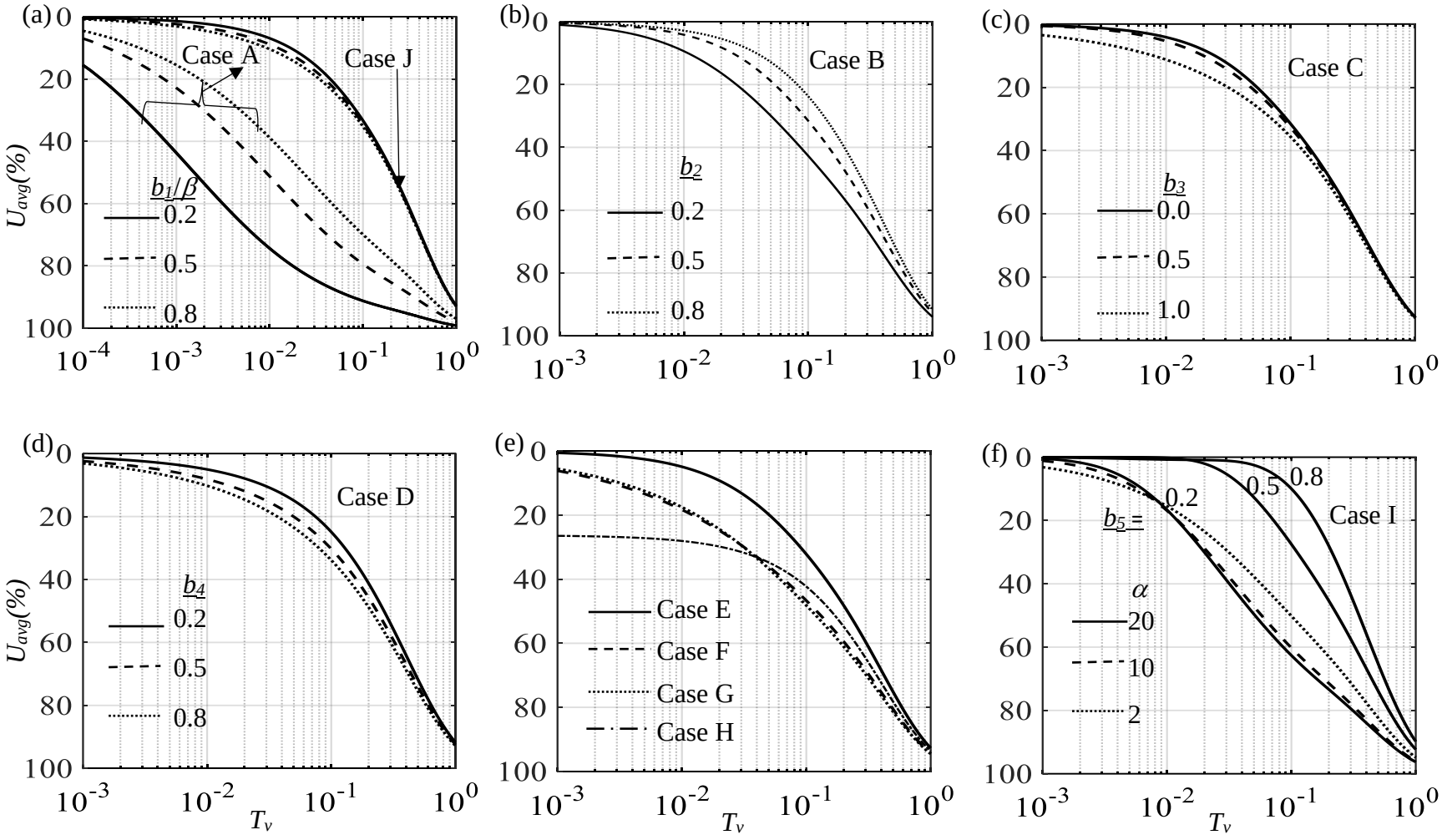

Fig. 3.8 U_{avg} versus T_v curves for the consolidating layer subjected to one-way drainage.

3.5 LAYERED SOIL

3.5.1 Problem Statement

A constant uniform load of magnitude q is applied over a horizontal surface of a clayey stratum consisting of two distinct layers, as shown in Fig. 3.9. The thickness of the top and the bottom layers are h_1 and h_2, respectively, and the layers are extended infinitely in lateral directions. The permeability and the compressibility characteristics within a particular layer are considered to be uniform and directionally independent. The consolidation of each layer is assumed to be governed by the one-dimensional linear diffusion equation. By considering different distributions of initial excess pore water pressure, it is intended to analyse the consolidation behaviour of the two-layered clays in terms of size and shape of the isochrones and consolidating curves. Corresponding to the different magnitude of h_1 and h_2 values, the analysis is performed for various combinations of compressible layers (e.g. soft over stiff/stiff over soft) and permeable layers (e,g, lower permeable over high permeable/high permeable over lower). The numerical solutions are obtained for same as previous boundary conditions.

3.5.2 NUMERICAL SCHEME

The consolidation behaviour of the multi-layered system can be expressed by the following canonical form:

Governing Differential Equation $$\frac{k_j}{\gamma_w m_{vj}} \frac{\partial^2 u}{\partial z^2} = \frac{\partial u}{\partial t} \tag{3.15}$$

Subjected to: (i) Boundary Constraint (Eqs. 3.11), (ii) Initial condition (Eq. 3.12),

(iii) an additional Interface Criterion: $$k_j \frac{\partial u}{\partial z} = k_{j+1} \frac{\partial u}{\partial z} \tag{3.16}$$

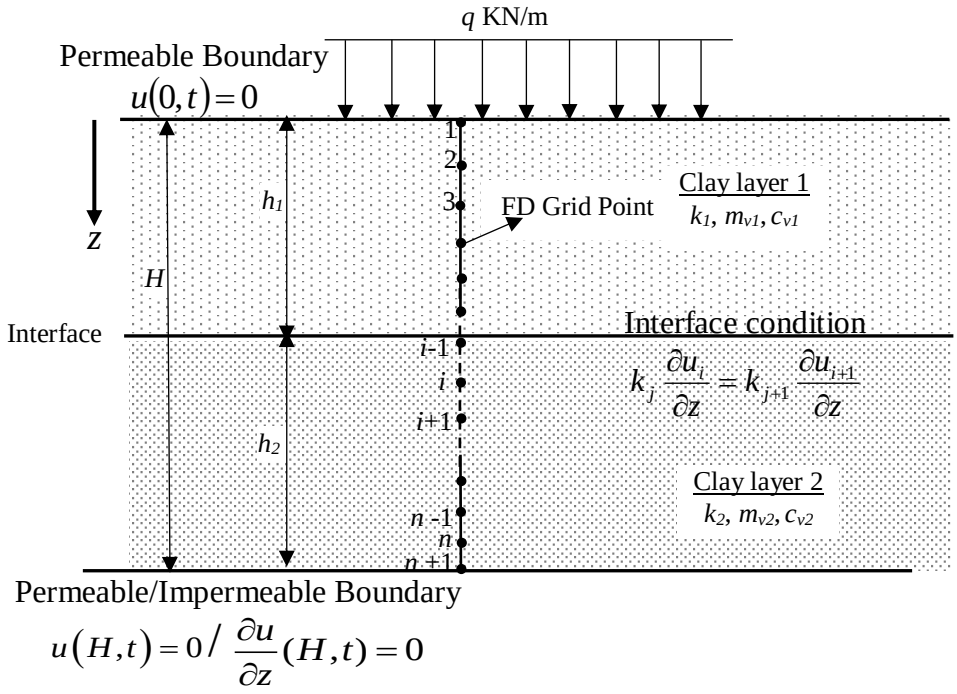

Fig. 3.9 Two-layered consolidating stratum subjected to strip loading along with the finite difference discretization.

where, (i) u is the excess PWP at any depth (z) corresponding to an arbitrary time (t), and, (ii) k_j and m_{vj} denotes the vertical permeability and the coefficient of volume compressibility of the j^{th} layer. The interface condition specified between two contiguous compressible layers eventually ensure that the quantity of flow from one layer equals the quantity of flow into the other layer. It is to be noteworthy that in contrast to the homogenous soil, the flow and the compressibility parameters are used distinctly.

Following the FD approach, Eq. (3.13) is discretized as the following form:

For 1st layer **:** $$\frac{u_i^{t+\Delta t}-u_i^t}{\Delta t}=c_{v1}\left(\frac{u_{i-1}^t-2u_i^t+u_{i+1}^t}{\Delta z^2}(1-\phi)+\frac{u_{i-1}^{t+\Delta t}-2u_i^{t+\Delta t}+u_{i+1}^{t+\Delta t}}{\Delta z^2}\phi\right) \quad (3.17)$$

At the interface**:**

$$\frac{1}{2\Delta t}\left[\frac{k_1}{c_{v1}}+\frac{k_2}{c_{v2}}\right]\left(u_i^{t+\Delta t}-u_i^t\right)=\frac{1}{2}\left[\frac{k_1}{\Delta z^2}+\frac{k_2}{\Delta z^2}\right]\times \left[\left\{\frac{2k_1}{k_1+k_2}u_{i-1}^{t+\Delta t}+\frac{2k_2}{k_1+k_2}u_{i+1}^{t+\Delta t}-2u_i^{t+\Delta t}\right\}\phi+\left\{\frac{2k_1}{k_1+k_2}u_{i-1}^{t}+\frac{2k_1}{k_1+k_2}u_{i+1}^{t}-2u_1^{t}\right\}(1-\phi)\right] \quad (3.18)$$

For 2nd layer: $\frac{u_i^{t+\Delta t}-u_i^t}{\Delta t}=c_{v2}\left(\frac{u_{i-1}^t-2u_i^t+u_{i+1}^t}{\Delta z^2}(1-\phi)+\frac{u_{i-1}^{t+\Delta t}-2u_i^{t+\Delta t}+u_{i+1}^{t+\Delta t}}{\Delta z^2}\phi\right)$ (3.19)

Re-arranging Eqs. (3.17), (3.18), and (3.19), the following three equations are formed:

$$-\lambda_1\phi\left(u_{i-1}^{t+\Delta t}-2u_i^{t+\Delta t}+u_{i+1}^{t+\Delta t}\right)+u_i^{t+\Delta t}=\lambda_1(1-\phi)\left(u_{i-1}^t-2u_i^t+u_{i+1}^t\right)+u_i^t \quad (3.20)$$

$$\mu\phi\left(\delta_1 u_{i-1}^{t+\Delta t}-2u_i^{t+\Delta t}+\delta_2 u_{i+1}^{t+\Delta t}\right)+u_i^{t+\Delta t}=\mu(1-\phi)\left(\delta_1 u_{i-1}^t-2u_i^t+\delta_2 u_{i+1}^t\right)+u_i^t \quad (3.21)$$

$$-\lambda_2\phi\left(u_{i-1}^{t+\Delta t}-2u_i^{t+\Delta t}+u_{i+1}^{t+\Delta t}\right)+u_i^{t+\Delta t}=\lambda_2(1-\phi)\left(u_{i-1}^t-2u_i^t+u_{i+1}^t\right)+u_i^t \quad (3.22)$$

Here, $\lambda_1=\frac{c_{v1}\Delta t}{2\Delta z^2}$; $\lambda_2=\frac{c_{v2}\Delta t}{2\Delta z^2}$ $\delta_1=\frac{2k_1}{k_1+k_2}$; $\delta_2=\frac{2k_2}{k_1+k_2}$; and $\mu=\frac{k_1+k_2}{\Delta z^2\left[\frac{k_1}{c_{v1}}+\frac{k_2}{c_{v2}}\right]}$

These finite difference form generates a simultaneous set of linear algebraic equations, as shown in Appendix A2. The loops run over time and at each time step, the excess PWP variables are updated by using the information of the previous time step. The step sizes are kept to be the same for both the layers. After performing several numerical analyses, it is noticed that the solutions obtained from different FD schemes are moderately different only at the initial stage of consolidation; after some phase of dissipation, the FD schemes do not influence the consolidation behaviour.

3.5.3 RESULTS AND DISCUSSIONS

The numerical solutions are plotted in terms of normalized isochrones, u_{max} path, consolidating curves (U_{avg} versus normalized time) and, the rate of dissipation ratio by varying the k_1/k_2, m_{v1}/m_{v2} and h_1/H ratios within a practical range.

3.5.3.1 Isochrones

Figs. 3.10-3.15 depict the isochrones for various two-layered clays; Figs. 3.10-3.12 and 3.13-3.15 indicate the curves for PTPB and PTIB conditions, respectively. The isochrones are presented in the normalized form due to non-uniformity of the u_0 distributions; here, u

and z axes are normalized with respect to the maximum value of u_0 ($u_{0,max}$) and thickness of the stratum (H), respectively. As the coefficient of consolidation (c_v) of two layers are different, therefore, the time factor (T_v) for each layer are not unique, and hence, unlike the conventional way of representation, the isochrones in the present chapter are drawn at a specific time but not at particular time factor.

Figs. 3.10 and 3.13 reveal the impact of the permeability ratio on the isochrones. Five different values of k_1/k_2, namely, 0.01, 0.1, 1.0, 10, and 100 are chosen for the purpose of illustration; the magnitude of $m_{v1}/\ m_{v2}$ (=1) and h_1/H (=0.3) are kept to be constant. It is observed that the curves pertaining to the layered soil deviate considerably from its homogenous counterpart, especially in the interface zone of the two layers. The curves associated with the high permeability ratio lies at the left side of the homogenous curves; this indicates that if high permeable clay lies over the lower permeable clay than the rate of dissipation increases significantly. It is also to be noted that the discrepancy between the isochrones originated from k_1/k_2=0.1(/10) and k_1/k_2=1 is strikingly high; however, the isochrones associated with k_1/k_2=0.01 (/100) deviate insignificantly from those generated from k_1/k_2=0.1(/10). It is important to note that the skewed and the arched distribution of u_0 accelerate the dissipation of excess PWP markedly. For single drained clays, the isochrones intersect the bottom impervious surface orthogonally. Near to the impervious surface, the pore water pressure curves shift rightward towards the u_0 curves (indicating the increase of excess PWP) up to a considerable amount of time. This is because of the redistribution of excess pore water pressure. Due to this phenomenon, Lovisa et al. (2010) suggested that the normalization of the isochrones with respect to $u_{0,max}$ is a better alternative for representing the consolidation behaviour. Although this redistribution is more prevalent for PTIB case, however, the increment of the excess PWP with time seems

to occur near the interface of the layered soil even for the doubly drained soil; especially, for the case where u_0 increases with depth (e.g. Cases D, H).

3.5.3.2 u_{max} path

Fig. 3.16 shows the u_{max} path by varying the apex position of the triangular (b_2) and skewed (b_5) u_0 loadings (Figs. 3.16a and 3.16b) and shorter base lengths (b_2 and b_3) of the trapezoidal u_0 distribution (Figs. 3.16c and 3.16d). These u_{max} paths are traced for three different m_{v1}/m_{v2} ratio (= 0.1, 1, 10) and one particular depth ratio (h_1/H = 0.3). From the figures, it can be deduced that whatever be the form of u_0 loadings, the u_{max} paths are unaffected by the change in m_{v1}/m_{v2} ratio if the drainage condition is PTIB type. However, the u_{max} paths generated from the double drained stratum are appreciably influenced by m_{v1}/m_{v2} ratio; especially, for triangular and trapezoidal u_0 loading. Similar to the homogenous clays, the u_{max} path for PTPB condition traverse almost the same path when the stiffer layer is laid over the softer layer.

After some phase of consolidation, the u_{max} paths corresponding to the PTPB condition and m_{v1}/m_{v2} =10 travels through the interface of the two layers no matter what the u_0 distribution is assumed. This trend is completely in contrast with the u_{max} paths originated from the stratum having m_{v1}/m_{v2} =0.1 or 1. The u_{max} path provides more clarity and flexibility for representing the progress of consolidation phenomenon with time corresponding to various drainage conditions, soil type and u_0 distributions in the same graph which otherwise would be clumsy and illegible if being done through the isochrones.

3.5.3.3 U_{avg} versus normalized time

Figs. 3.17-3.20 represent the variation of average degree of consolidation (U_{avg}) with normalized time (t/t_o); Figs. 3.17-3.18. and 3.19-3.20. correspond to PTPB and PTIB conditions, respectively.

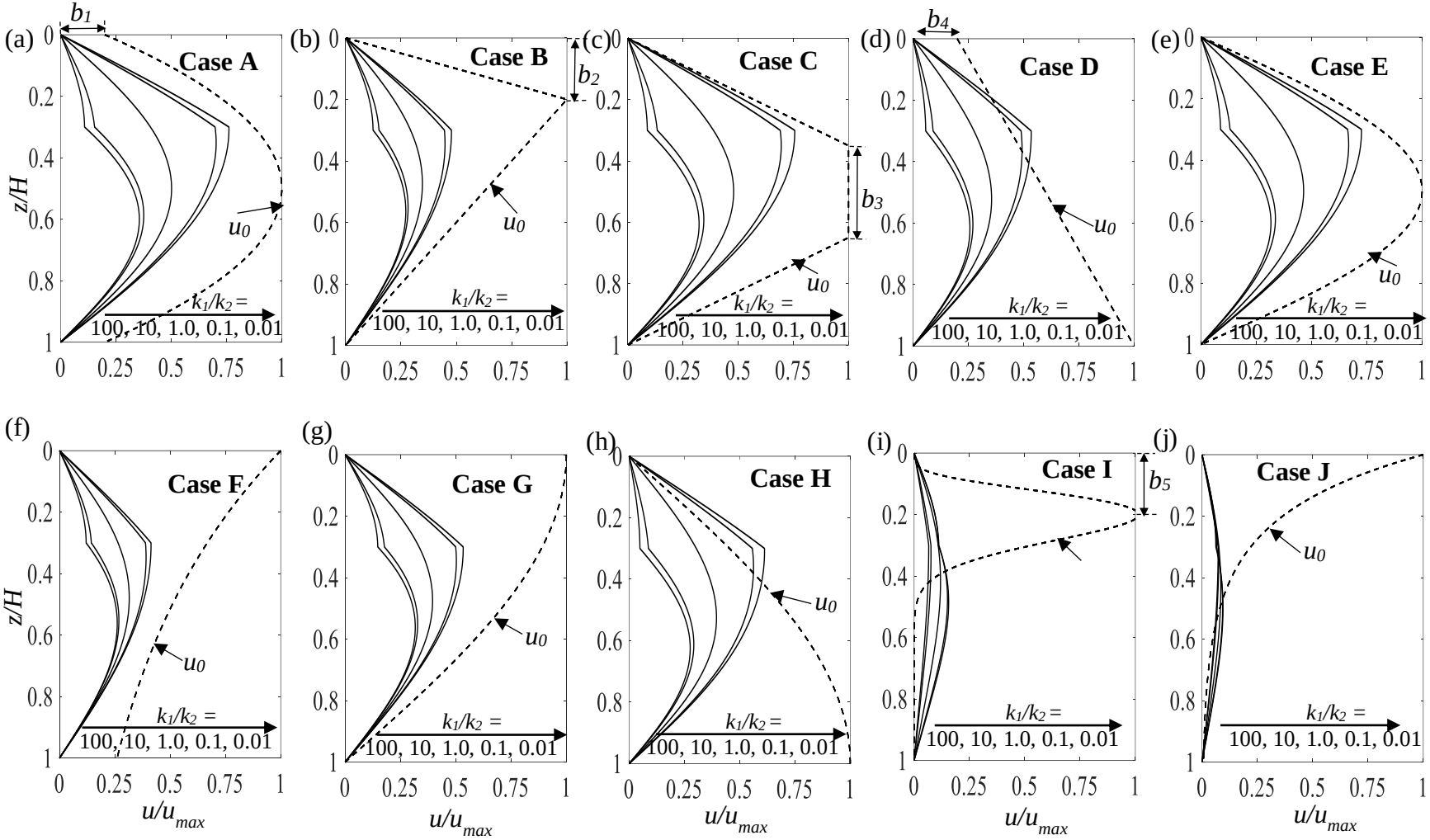

Fig. 3.10 Corresponding to various initial excess PWP distributions, the variation of normalized isochrones for different k_1/k_2 ratios having $m_{v1}/m_{v2} = 1$, $h_1/H = 0.3$ and subjected to two-way drainage.

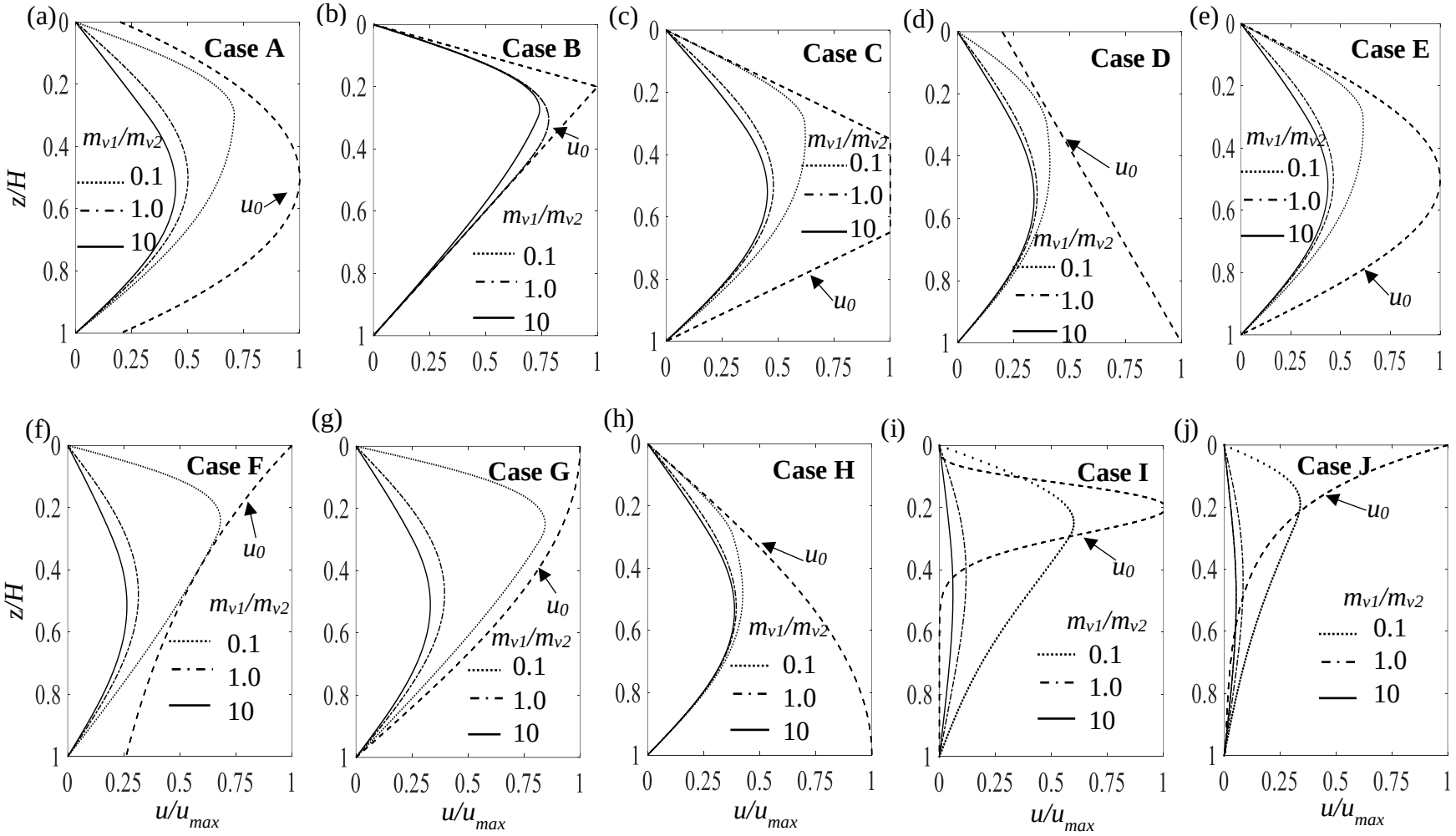

Fig. 3.11 Corresponding to various initial excess PWP distributions, the variation of normalized isochrones for different m_{v1}/m_{v2} ratios having $k_1/k_2 = 1$, $h_1/H = 0.3$ and subjected to two-way drainage.

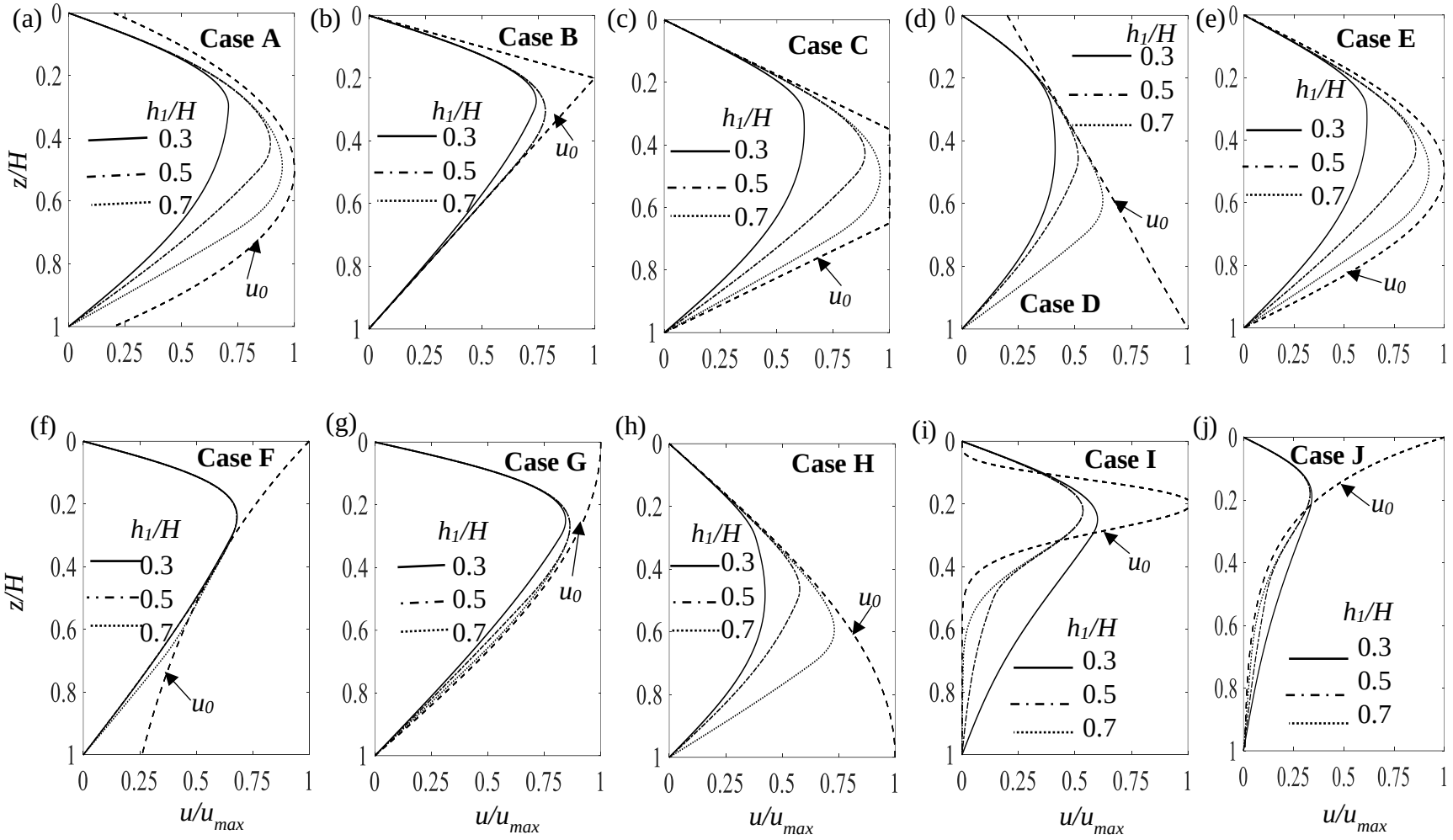

Fig. 3.12 Corresponding to various initial excess PWP distributions, the variation of normalized isochrones for different h_1/H ratios having $k_1/k_2 = 1$, $m_{v1}/m_{v2} = 10$ and subjected to two-way drainage.

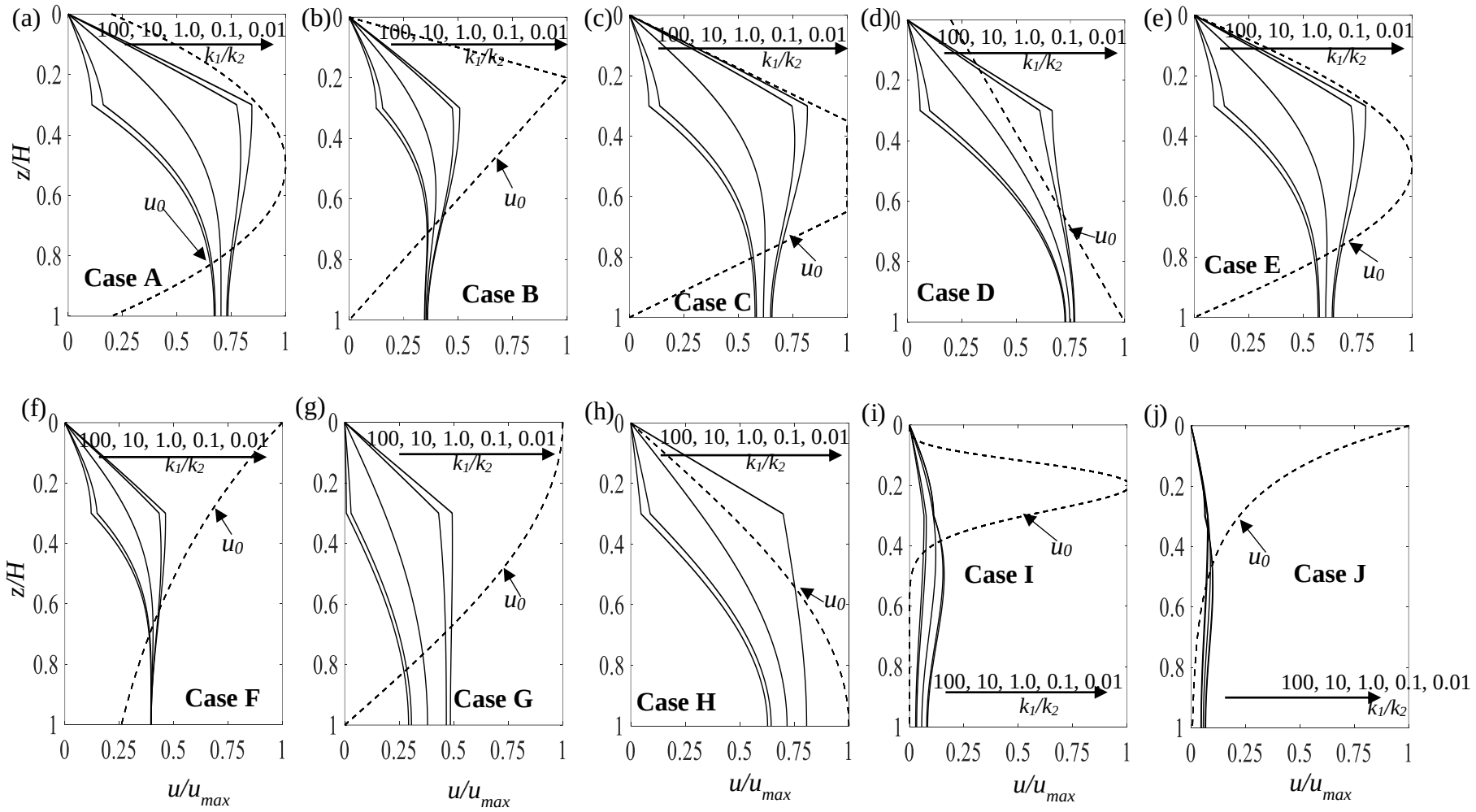

Fig. 3.13 Corresponding to various initial excess PWP distributions, the variation of normalized isochrones for different k_1/k_2 ratios having $m_{v1}/m_{v2} = 1$, $h_1/H = 0.3$ and subjected to one-way drainage.

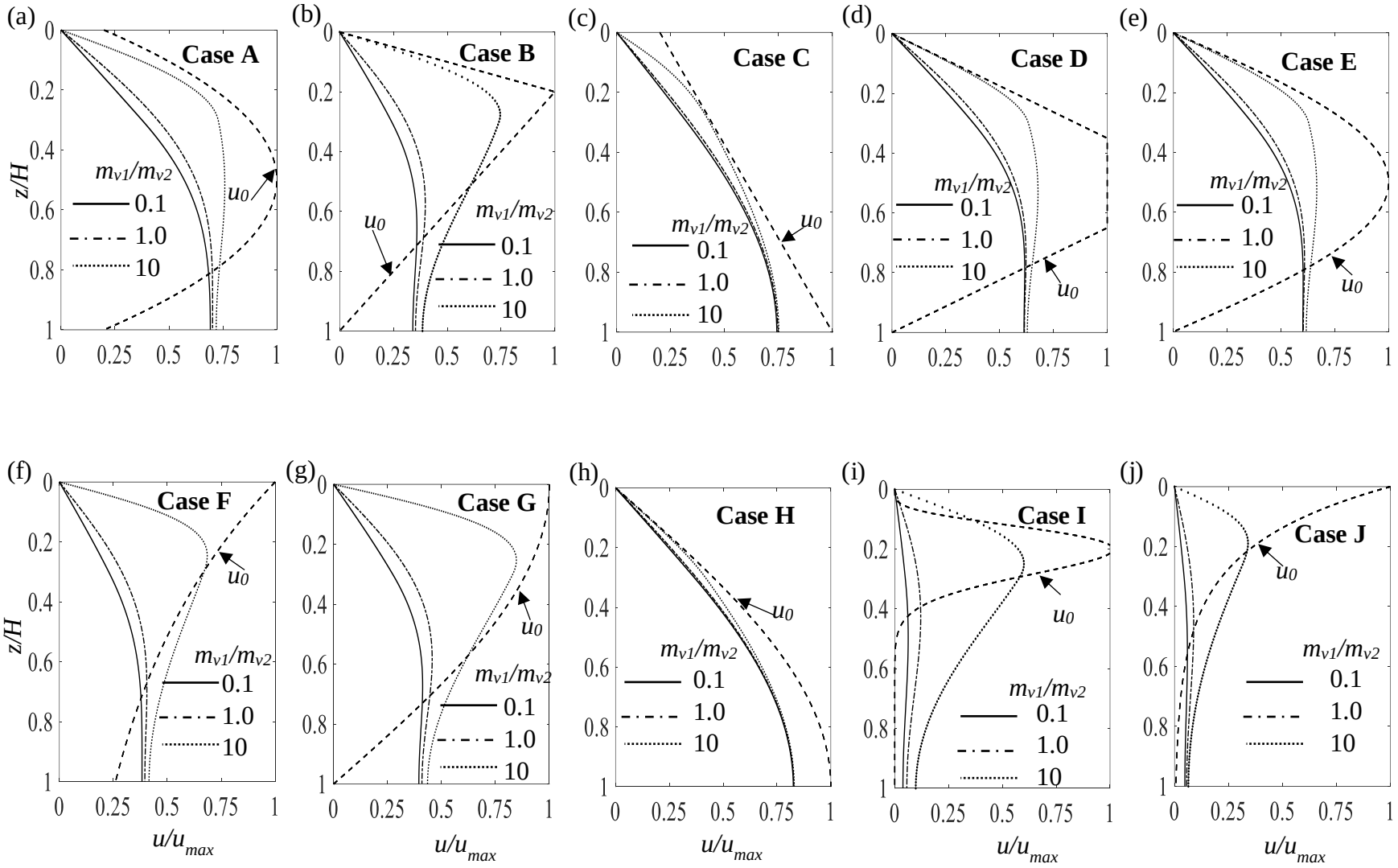

Fig. 3.14 Corresponding to various initial excess PWP distributions, the variation of normalized isochrones for different m_{v1}/m_{v2} ratios having $k_1/k_2 = 1$, $h_1/H = 0.3$ and subjected to one-way drainage.

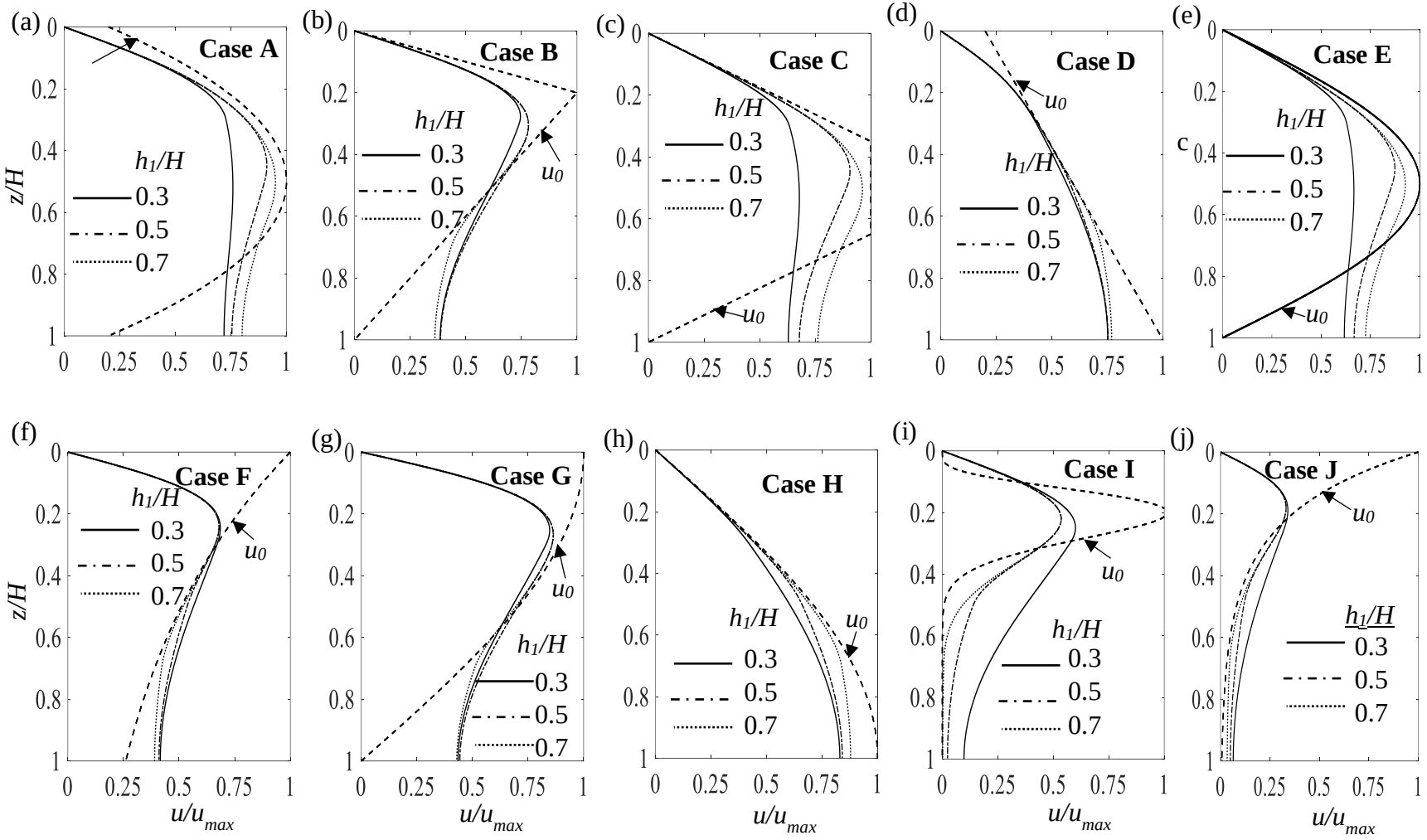

Fig. 3.15 Corresponding to various initial excess PWP distributions, the variation of normalized isochrones for different h_1/H ratios having $k_1/k_2 = 1$, $m_{v1}/m_{v2} = 10$ and subjected to one-way drainage.

Hence, these curves are referred as the consolidating curves or the settlement curves. Figs. 3.17 and 3.19 depict the impact of the permeability of the top layer on controlling the trend of the rate of consolidation settlement. The difference of the settlement curves obtained from the homogenous and the heterogeneous soil appears to be quite significant especially for the one-way drainage. In addition to that, the difference between the settlement curves associated with k_1/k_2 = 10 and k_1/k_2 = 100 was marginal for both the drainage condition; whereas, the curves correspond to k_1/k_2 = 0.01 and k_1/k_2 = 0.1 are quite apart for one-way drainage. If most of the initial excess PWP is assumed to develop near the top surface of the clayey stratum (Case B, F, G, I, J) then the settlement curves intersect each other after some phase of the consolidation process for both the drainage conditions. This gives an impression that even if the average vertical permeability of a clayey stratum is more, however, that does not guarantee in faster dissipation of excess PWP. For few specific u_0 distributions (Case D, H, I) placing a very low permeable soil over the higher one results in the formation of a hump in the consolidation curves, especially for the PTIB case; this, in a sense, indicates an expansion of the consolidating layer. It may be possible that due to small k_1/k_2 ratio and of imperviousness of the bottom surface, water cannot easily drain out from the top layer and might cause the accumulation of water near the top layer which eventually results in the expansion of the soil. The influence of the compressibility and the depth ratios on the settlement curves are presented in Figs. 3.18 and 3.20. In contrast to the horizontal stratum (i.e. m_{v1}/m_{v2} =1), an insignificant difference seems to observe in the settlement curve obtained from lower m_{v1}/m_{v2} ratio. On the contrary, higher m_{v1}/m_{v2} ratio impacts the consolidation curves significantly; especially, for those asymmetric u_0 distributions which decrease with depth as shown in Case B, F and G; for such u_0 loadings, the consolidation curves inflate for certain time duration corresponding to PTIB condition. The graphs in Figs. 3.18i and 3.20i indicate that the assumption of skewed distribution of

u_0 would results in a negative U_{avg} for those clayey strata where a very high compressible layer is placed over the stiff layer.

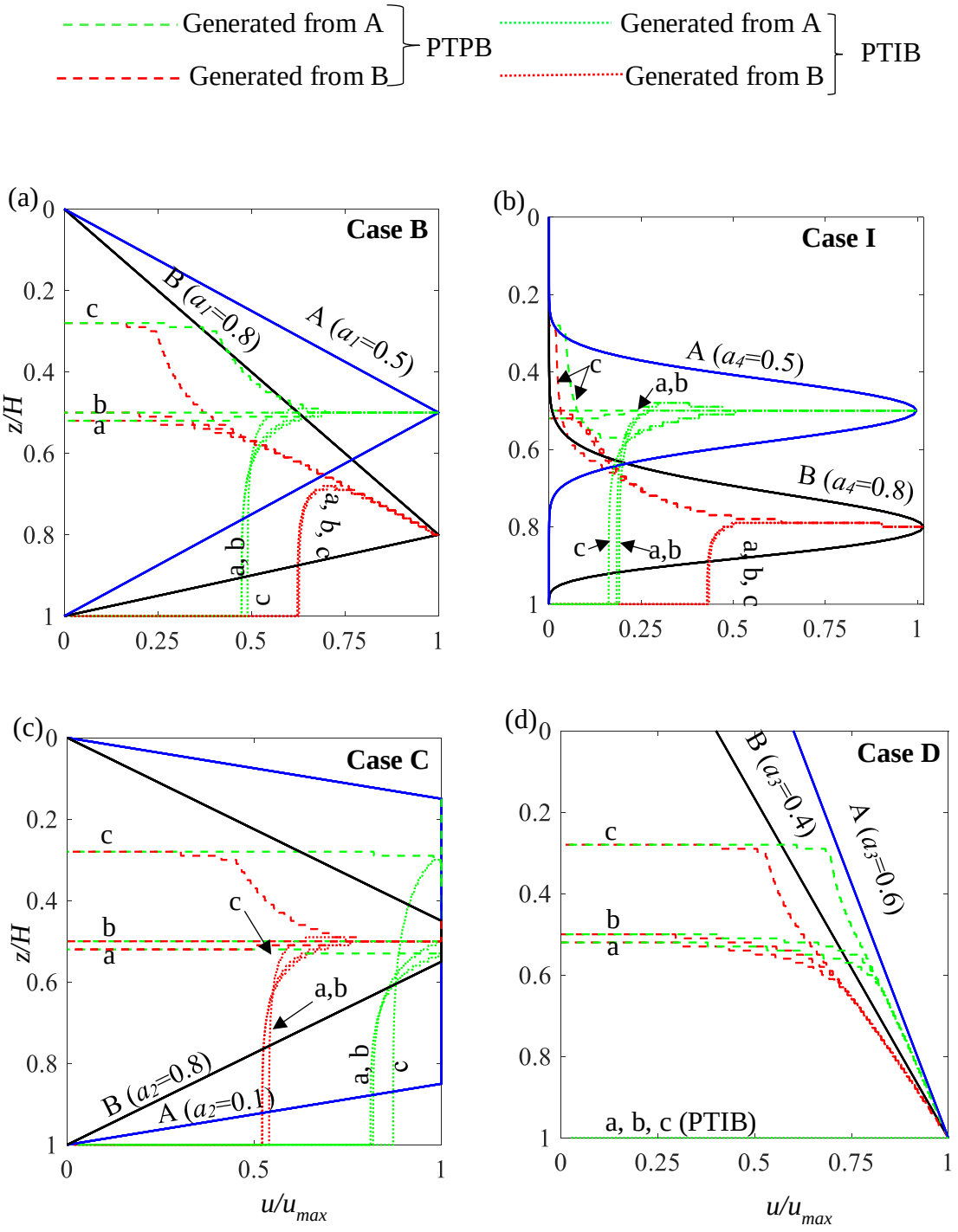

N.B.: (i) a, b, c represents m_{v1}/m_{v2} equals to 0.1,1, and 10 respectively.

(ii) h_1/H = 0.3 and k_1/k_2 =1.

Fig. 3.16 Variation of u_{max} path by changing the controlling parameters of four u_o distributions: (a) Case B, (b) Case I, (b) Case C, and, (b) Case D.

The reason can be attributed to the fact that at some phase of consolidation the area enclosed within the isochrone is larger than the area made by the skewed u_0 distributions. The event of these expansions is far more significant for one-way drainage condition. As the thickness of the top layer (soft) increases, the rate of dissipation reduces regardless of the drainage conditions. This feature can be explained from the previous inference that increasing the compressibility of the softer layer delays the process of consolidation. However, the skewed and the arched distribution shows the reverse trend maybe because of the predominance of the effect of redistribution of the excess PWP.

3.5.3.4 Rate of dissipation with time

Following Lovisa and Sivakugan (2014), the difference of the dissipation rate between any assumed non-uniform u_0 distribution with the conventional rectangular u_0 distribution is compared through rate of dissipation ratio (*RDR*). *RDR* is defined as follows:

$$RDR=R_1/R_0 \tag{3.23}$$

where, R_1 and R_0 denote the normalized area of undissipated excess PWP attained at any arbitrary time during consolidation for non-uniform and uniform u_0 distribution, respectively and is expressed as follows:

$$R_1 = \frac{\left[\int_0^H u(z,t)\,dz\right]_{non-uniform}}{\left[\int_0^H u(z,0)\,dz\right]_{non-uniform}} \quad ; \quad R_0 = \frac{\left[\int_0^H u(z,t)\,dz\right]_{uniform}}{\left[\int_0^H u(z,0)\,dz\right]_{uniform}} \tag{3.24}$$

Figs. 3.21 and 3.22 show the trend of *RDR* with respect to time for PTPB and PTIB conditions, respectively. These graphs give the idea of how fast (or slow) the process of consolidation progresses with time if the initial excess PWP is developed non-uniformly instead of the conventional assumed uniform distribution.

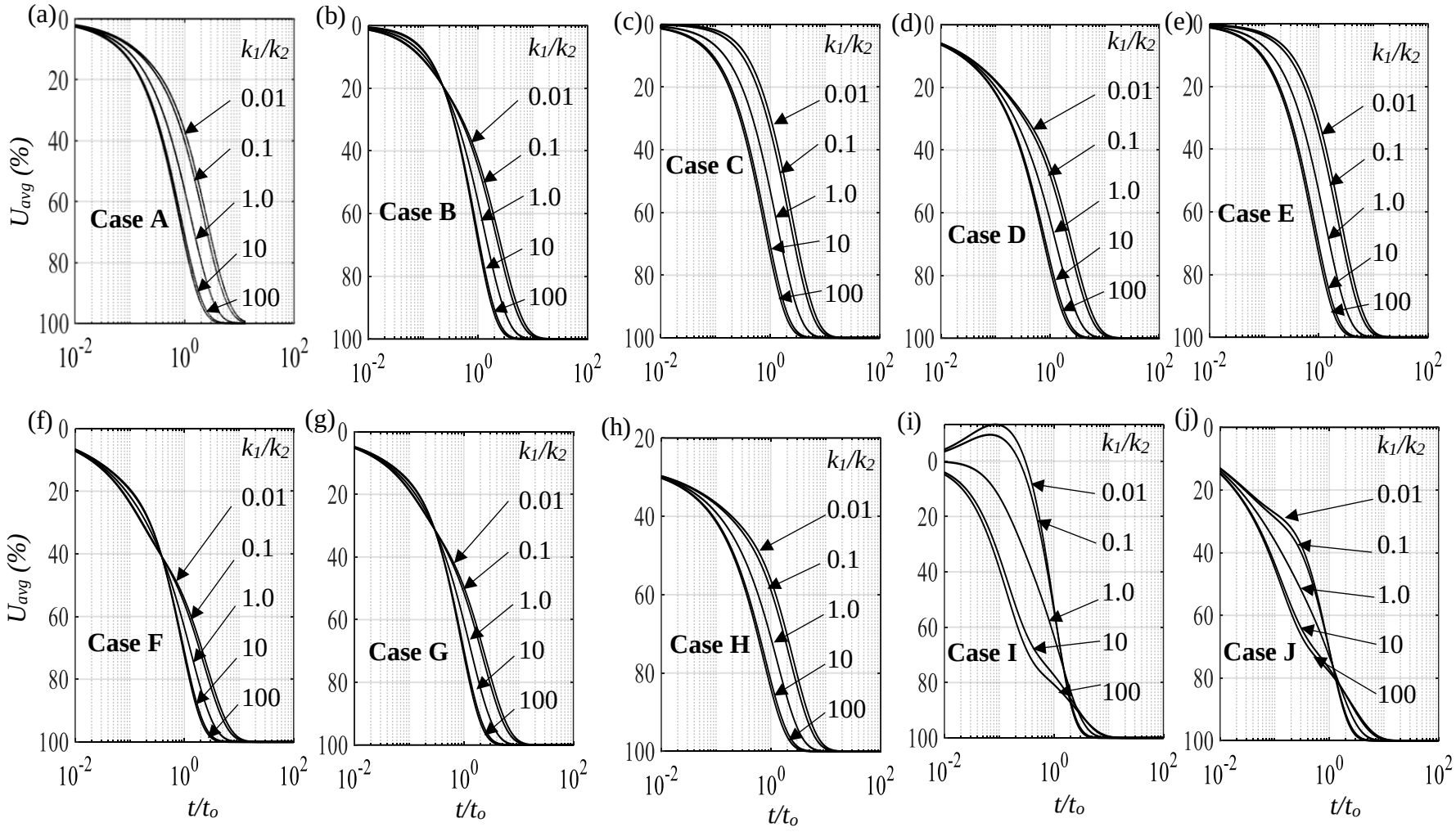

Fig. 3.17. Corresponding to various initial excess PWP distributions, the variation of U_{avg} with respect to normalized time for different k_1/k_2 ratios having $m_{v1}/m_{v2} = 1$, $h_1/H = 0.3$ and subjected to two-way drainage.

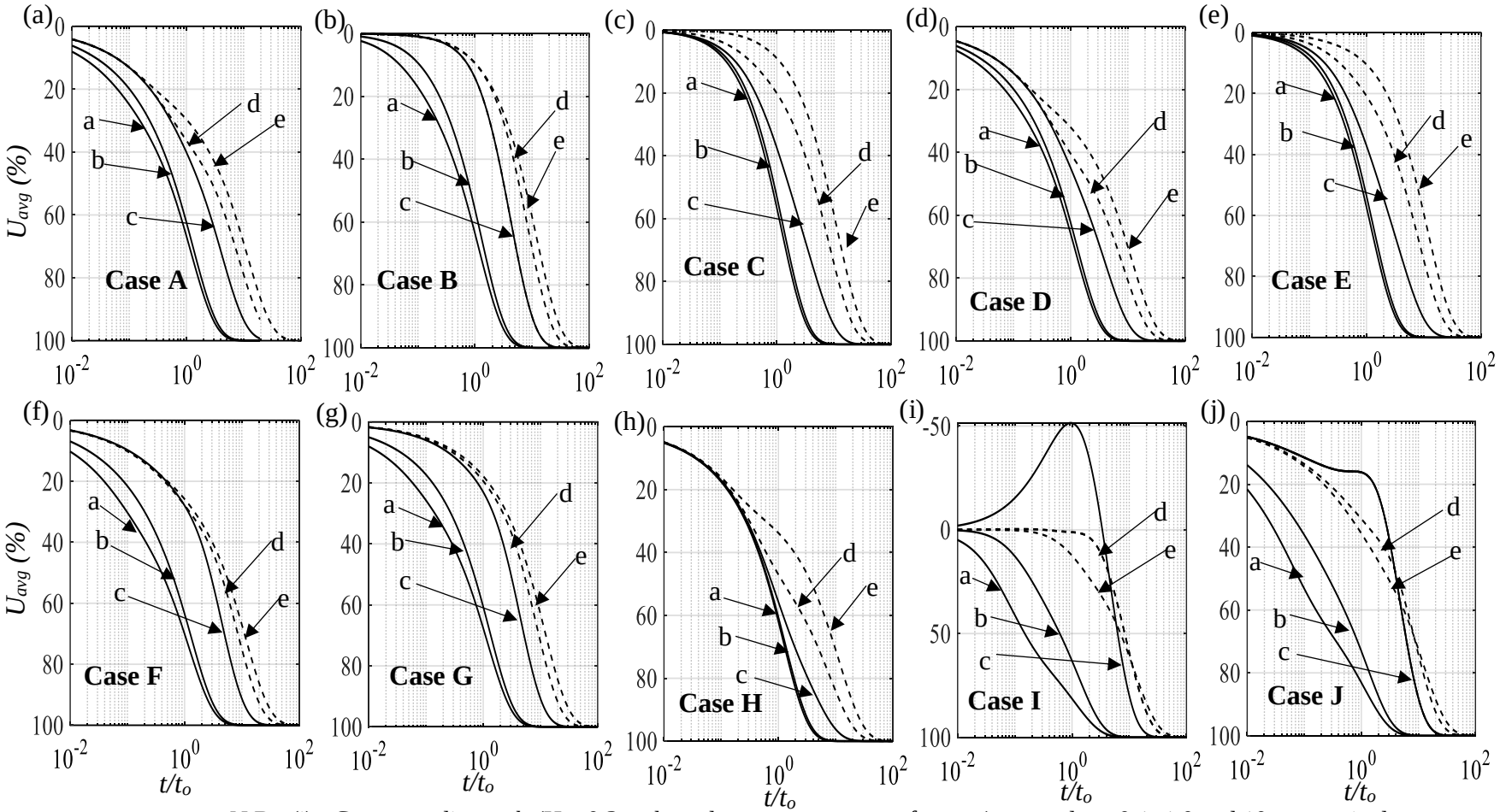

N.B.: (i) Corresponding to h_1/H = 0.3, a, b, and c represent curves for m_{v1}/m_{v2} equals to 0.1, 1.0 and 10, respectively.

(ii) Corresponding to m_{v1}/m_{v2} = 10, d and e represent curves for h_1/H equal to 0.5 and 0.7, respectively.

Fig. 3.18. Corresponding to various initial excess PWP distributions, the variation of U_{avg} with respect to normalized time for different m_{v1}/m_{v2} and h_1/H ratios having k_1/k_2 = 1, and subjected to two-way drainage

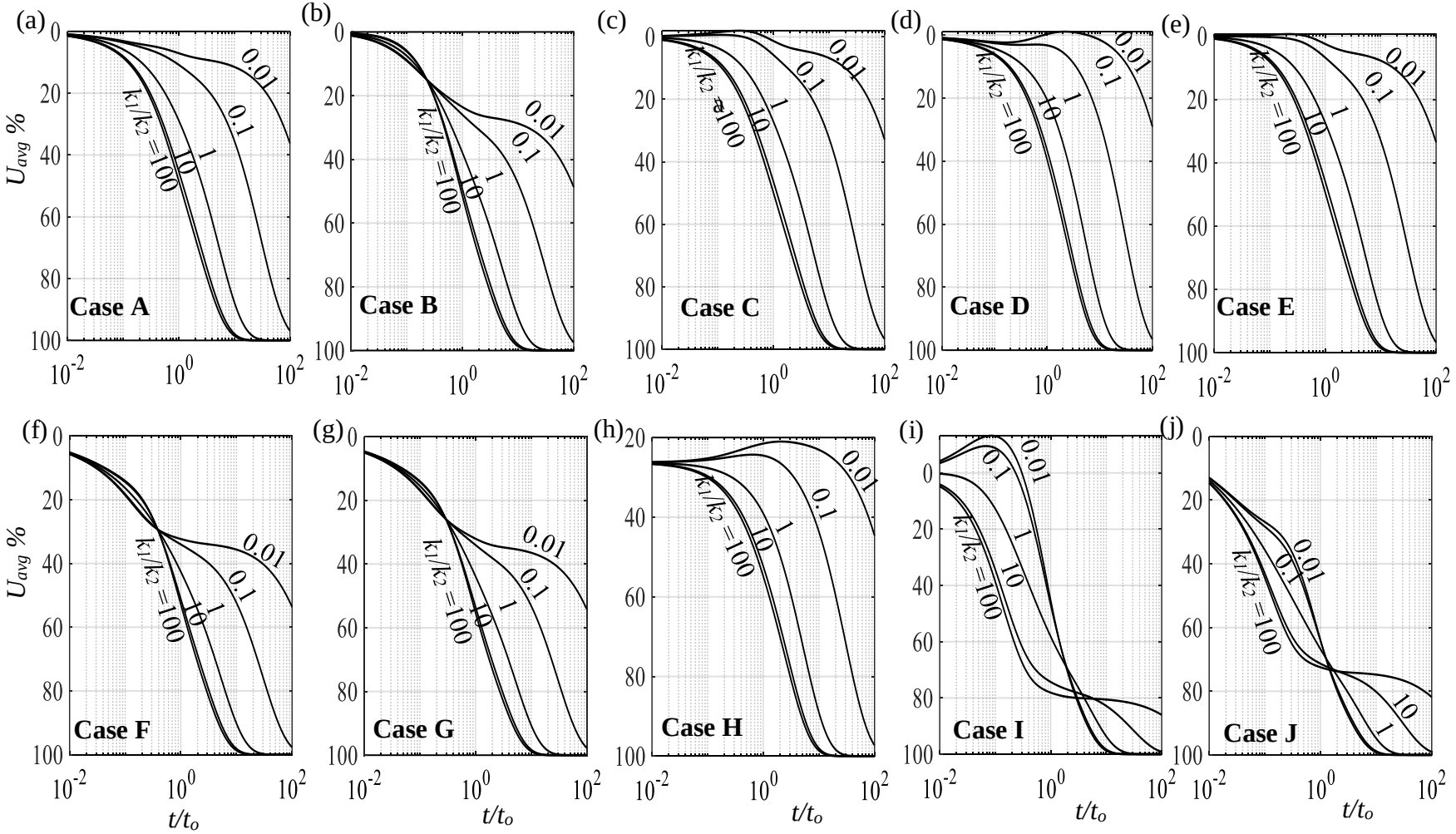

Fig. 3.19. Corresponding to various initial excess PWP distributions, the variation of U_{avg} with respect to normalized time for different k_1/k_2 ratios having m_{v1}/m_{v2} = 1, h_1/H = 0.3 and subjected to one-way drainage

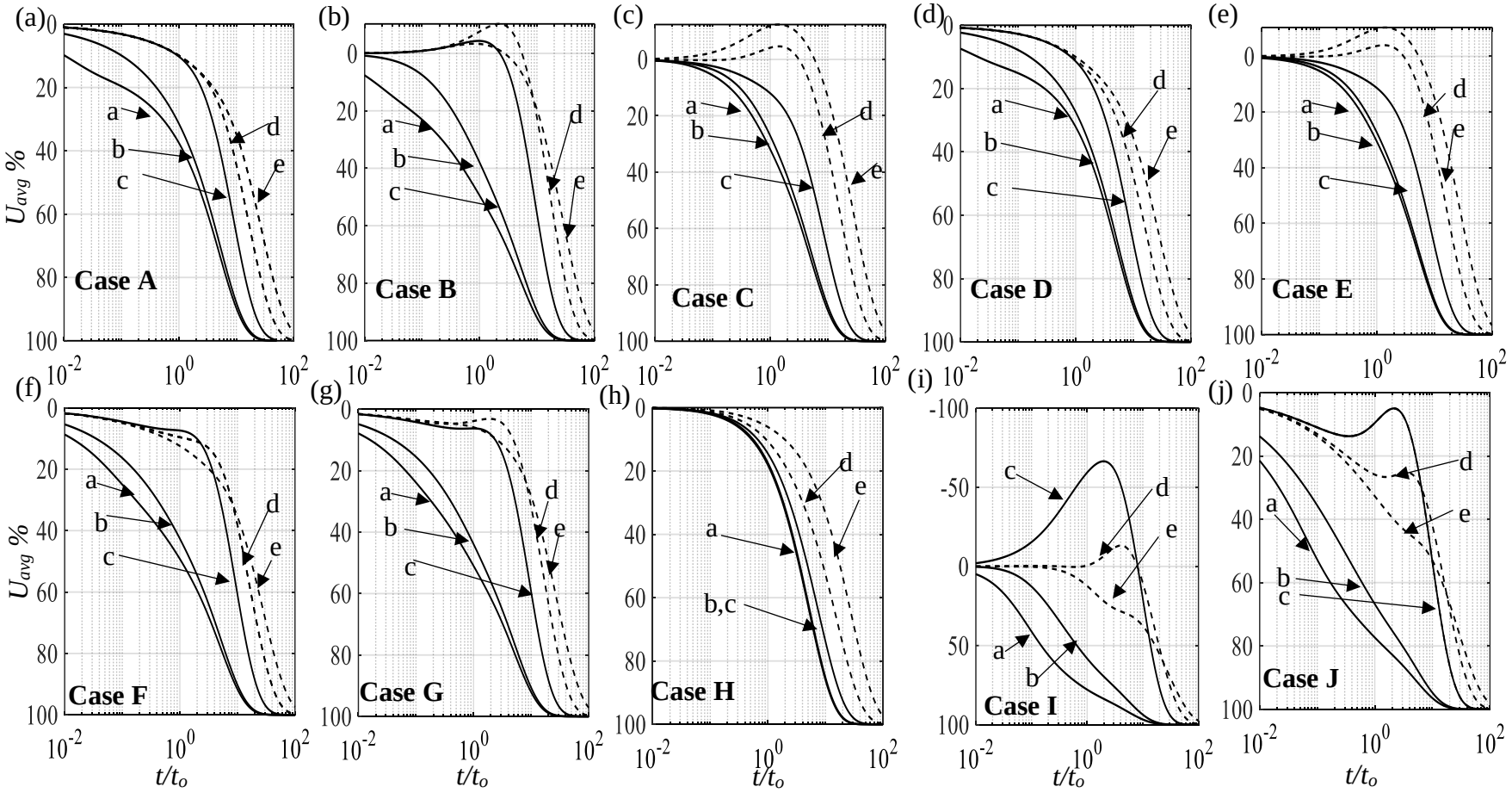

N.B.: (i) Corresponding to h_1/H = 0.3, a, b and c represent curves for m_{v1}/m_{v2} equals to 0.1, 1.0 and 10, respectively.

(ii) Corresponding to m_{v1}/m_{v2} = 10, d and e represent curves for h_1/H equal to 0.5 and 0.7, respectively.

Fig. 3.20. Corresponding to various initial excess PWP distributions, the variation of U_{avg} with respect to normalized time for different m_{v1}/m_{v2} and h_1/H ratios having k_1/k_2 = 1, and subjected to one-way drainage.

The figures are plotted for two different k_1/k_2 (r) (=0.01 and 100) corresponding to two different values of m_{v1}/m_{v2} (p), namely, 0.1 and 10. It is clearly seen that the variation of *RDR* depends highly on the (i) assumed u_0 distribution, (ii) layer properties and (iii) drainage conditions. It can be deduced from the graphs that for a clay stratum subjected to two-way drainage system and consisting of high compressible layer over low compressible layer (and/or high permeable over low permeable), the magnitude of *RDR* is (i) greater than unity for Cases B, F, G and I and (ii) smaller than unity for Cases D and H. For these asymmetric u_0 loadings, if the permeability and the compressibility parameters of the layers are altered, the variation of *RDR* shows a reverse trend. Except the curves related to k_1/k_2 =100, the trend of all other curves appears to be similar even for the one-way drainage condition. For the symmetric u_0 distribution (Cases C and E), the variation of *RDR* with time is similar for both the drainage conditions.

3.6 VALIDATION

Table 3.1. shows the comparison between the present numerical solutions with the analytical results provided by (Lovisa et al.2010; 2012) for various assumptions of the u_0 distribution. The comparison is made on the basis of U_{avg} value corresponding to both the drainage conditions. Due to non-availability of the solutions for two-layered clays subjected to constant loading and various u_0 distributions, the comparison is carried out solely for the homogenous soil. For most of the cases, the obtained values are in well agreement with the analytical results even up to two decimals. Fig 3.23a depicts the comparison of the isochrones with the solutions provided by Lambe and Whitman (1969) for triangular u_0 loadings corresponding to double drainage conditions. The present solutions match quite well with the analytical solutions of Lambe and Whitman (1969).

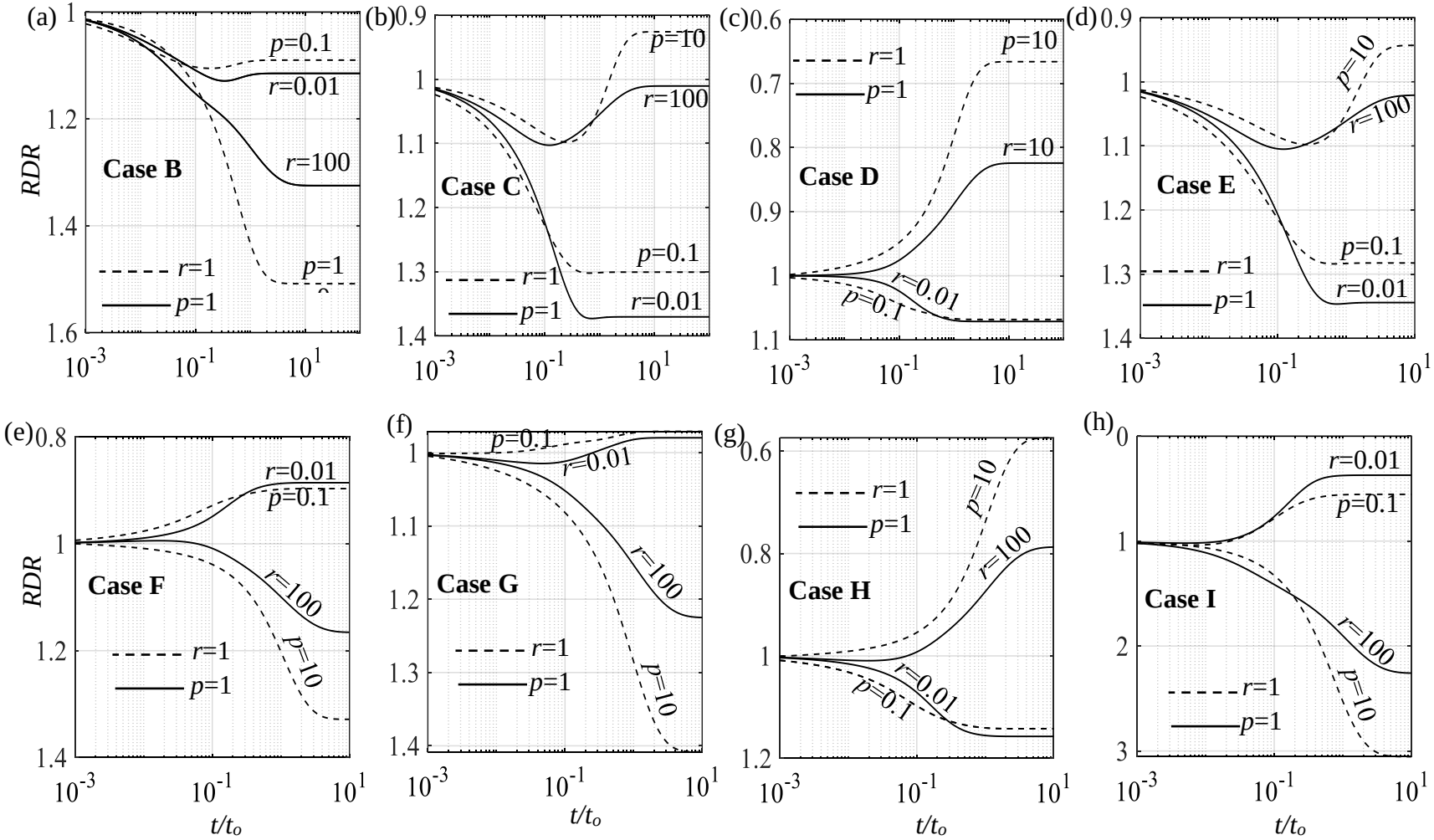

Fig. 3.21. Variation of *RDR* with respect to normalized time for different combinations of k_1/k_2 (r) and m_{v1}/m_{v2} (p), corresponding to h_1/H=0.3, and subjected to PTPB drainage conditions and various u_0 loadings.

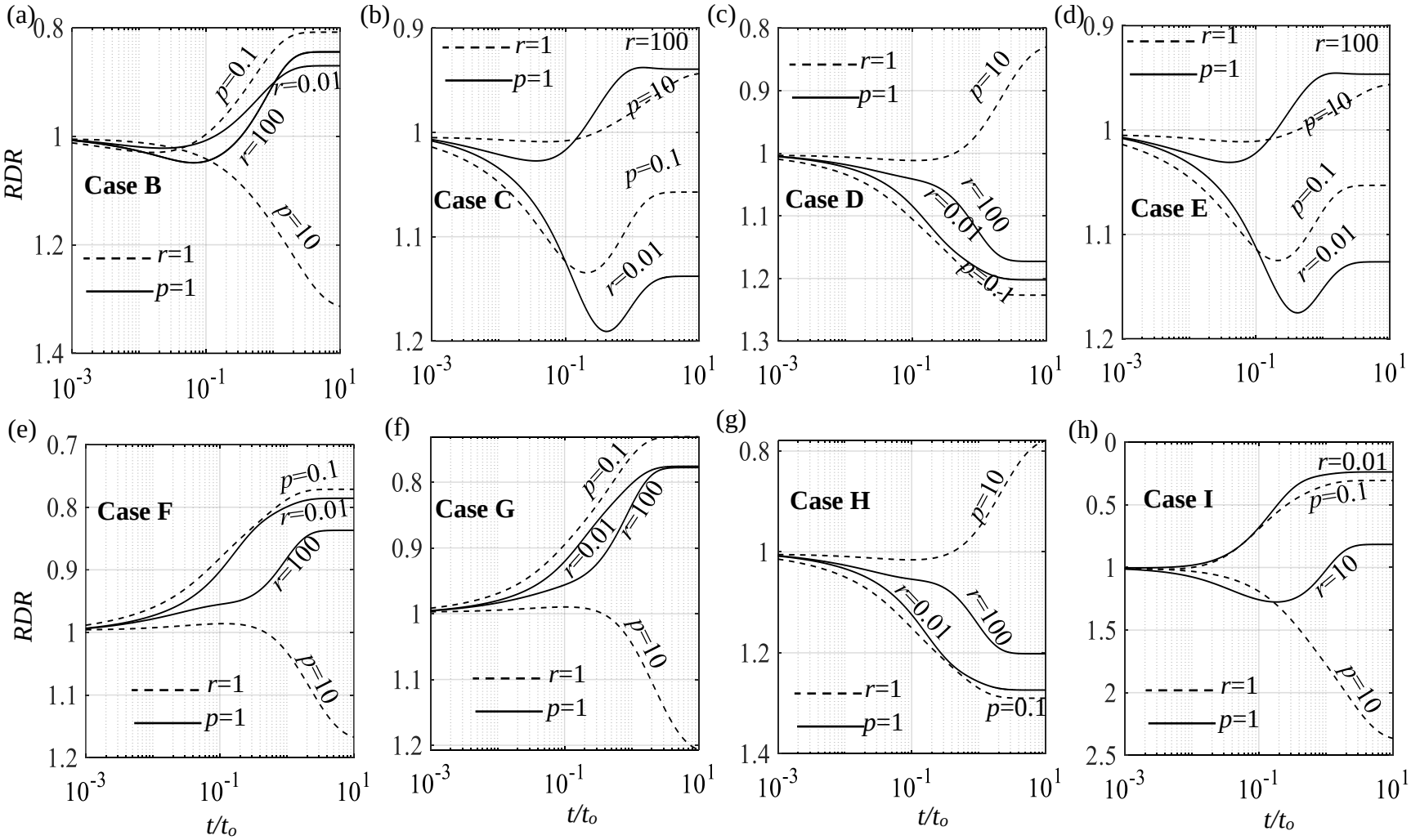

Fig. 3.22. Variation of *RDR* with respect to normalized time for different combinations of k_1/k_2 (r) and m_{v1}/m_{v2} (p), corresponding to h_1/H=0.3, and subjected to PTIB drainage conditions and various u_0 loadings.

Table 3.1. A comparison of the present numerical solutions with the analytical solutions presented by Lovisa et al. (2010; 2012).

			z/H = 0.2		*z/H* = 1.0		*z/H* = 1.8	
		T_v	Present results	Lovisa et al. (2010)	Present results	Lovisa et al. (2010)	Present results	Lovisa et al.(2010)
PTPB	Case D (b_4= 0.2)	0.10	0.145	0.149	0.569	0.569	0.264	0.265
		0.20	0.125	0.125	0.456	0.463	0.165	0.167
		0.30	0.099	0.105	0.364	0.364	0.125	0.120
	Case B (b_2=0.5)	0.10	0.185	0.187	0.642	0.643	0.192	0.187
		0.20	0.152	0.152	0.496	0.496	0.152	0.152
		0.30	0.119	0.119	0.384	0.387	0.125	0.119
	Case E	0.10	0.231	0.241	0.774	0.781	0.245	0.241
		0.20	0.178	0.188	0.602	0.610	0.185	0.188
		0.30	0.145	0.147	0.476	0.477	0.152	0.147
			z/H = 0.2		*z/H* = 0.6		*z/H* = 1.0	
			Present results	Lovisa et al. (2012)	Present results	Lovisa et al. (2012)	Present results	Lovisa et al. (2012)
PTIB	Case D (b_4=0.2)	0.10	0.221	0.219	0.565	0.572	0.697	0.707
		0.20	0.168	0.171	0.455	0.447	0.546	0.554
		0.30	0.131	0.133	0.349	0.350	(0.428	0.434
	Case B (b_2= 0.5)	0.02	0.361	0.376	0.652	0.648	0.333	0.308
		0.06	0.262	0.267	0.510	0.506	0.452	0.459
		0.10	0.191	0.199	0.425	0.437	0.472	0.473
	Case E	0.02	0.493	0.461	0.798	0.797	0.488	0.430
		0.06	0.348	0.346	0.653	0.635	0.606	0.587
		0.10	0.273	0.248	0.564	0.551	0.600	0.603

It is noteworthy that in the present chapter, the continuity conditions of the primary and the secondary (first order) variables on *u* at the interface are strictly maintained. However, back in sixties, U.S. Navy (1962) provided a simple recommendation to deal with two-layered clays with double drainage. They proposed two separate stages for evaluating the consolidation: (a) first the more permeable layer with PTIB condition and (b) then the less permeable layer with two-way drainage. Solution charts of this approximate method are not available for further comparisons. Due to non-

availability of the solutions for two-layered clays subjected to constant loading and various u_0 distributions, a comparison is carried out with the early work of Luscher (1965) considering uniform u_0 distributions. Fig 3.23b presents such comparisons. The closeness of the solutions provides adequate confidence in the reported values obtained from the present computation.

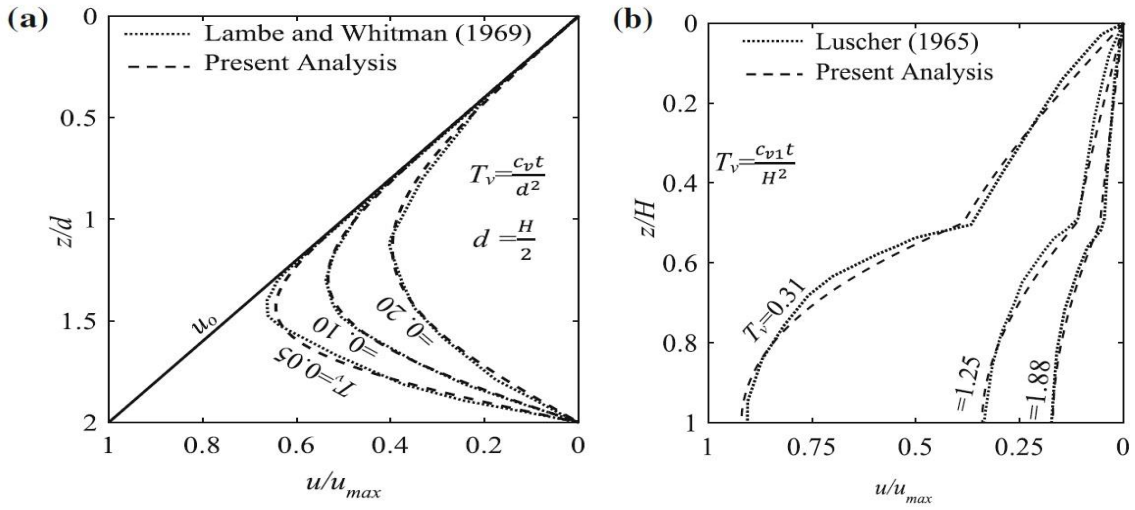

Fig. 3.23 Comparisons of the present solutions with the solutions provided for **(**a) homogenous soil (Lambe and Whitman, 1969) and **(**b) layered soil (Luscher, 1965)

3.7 SUMMARY

The analysis reveals that the dissipation process of the consolidating layer (homogeneous and two-layered) is significantly affected by the shape of u_0 distributions. The study is conducted by employing the Crank Nicolson semi-implicit scheme of the finite difference scheme. The results are presented in terms of normalized isochrones, consolidating curves, and a newly developed approach "u_{max} path" for both one-way as well as two-way drainage boundary condition. The u_{max} path shows how the position of the maximum pore water pressure in the clayey layer varies with time. This approach seems to be more efficient in representing the comparative behavior of the consolidation phenomenon. The analyses reveal that the forms of the assumed u_0 distribution impact the consolidation phenomenon immensely.